PCCP

Cite this: *Phys. Chem. Chem. Phys.*, 2012, **14**, 11245–11267

www.rsc.org/pccp

PERSPECTIVE

Alignment of electronic energy levels at electrochemical interfaces

Jun Cheng and Michiel Sprik*

Received 21st May 2012, Accepted 18th June 2012
DOI: 10.1039/c2cp41652b

The position of electronic energy levels in a phase depends on the surface potentials at its boundaries. Bringing two phases in contact at an interface will alter the surface potentials shifting the energy levels relative to each other. Calculating such shifts for electrochemical interfaces requires a combination of methods from computational surface science and physical chemistry. The problem is closely related to the computation of potentials of electrochemically inactive electrodes. These so-called ideally polarizable interfaces are impossible to cross for electrons. In this perspective we review two density functional theory based methods that have been developed for this purpose, the workfunction method and the hydrogen insertion method. The key expressions of the two methods are derived from the formal theory of absolute electrode potentials. As an illustration of the workfunction method we review the computation of the potential of zero charge of the Pt(111)–water interface as recently published by a number of groups. The example of the hydrogen insertion method is from our own work on the rutile TiO_2(110)–water interface at the point of zero proton charge. The calculations are summarized in level diagrams aligning the electronic energy levels of the solid electrode (Fermi level of the metal, valence band maximum and conduction band minimum of the semiconductor) to the band edges of liquid water and the standard potential for the reduction of the hydroxyl radical. All potentials are calculated at the same level of density functional theory using the standard hydrogen electrode as common energy reference. Comparison to experiment identifies the treatment of the valence band of water as a potentially dangerous source of error for application to electrocatalysis and photocatalysis.

1 Introduction

Dipping a piece of metal into an electrolytic solution creates an interface between an electronic and ionic conductor. The electronic conductor together with its interface with the solution is what constitutes an electrode. An electrochemical experiment probes the properties of electrochemical interfaces by measuring the voltages and currents between two such electrodes under a variety of conditions.[1] Modelling is absolutely crucial to the understanding of the rather convoluted information in current–voltage plots. These models are formulated in terms of kinetic

Department of Chemistry, University of Cambridge, Lensfield Road, CB2 1EW Cambridge, UK. E-mail: ms284@cam.ac.uk

Jun Cheng

Jun Cheng studied chemistry under the supervision of Prof. Peijun Hu at Queen's University, Belfast, and received his PhD degree in 2008. He then moved to the University of Cambridge to work as a postdoctoral research associate in the group of Prof. Michiel Sprik. Since 2010, he has been a junior research fellow at Emmanuel College at Cambridge. His research in general is to simulate chemical processes at solid–gas and solid–liquid interfaces using ab initio methods, and the topics of interest include electrochemistry and catalysis.

Michiel Sprik

Michiel Sprik is a professor of Theoretical Chemistry at the University of Cambridge. He received his PhD in Physics from the University of Amsterdam in 1982. After an extended period as post-doctoral fellow in Canada and the United States he joined the computational group at IBM's Zurich Research Laboratory in 1990 from where he moved to Cambridge in 1998. He has a continuing interest in computational physical chemistry. The methods he is using have shifted over the years from force field based to density functional theory based molecular dynamics.

and transport equations and take a prominent place in textbooks on electrochemistry.[1–4] Providing an microscopic basis for these models from first principles remains a formidable challenge. Significant progress could be made using cluster models[5–9] or by parametrizing model hamiltonians using input from electronic structure calculations.[10–12]

If first principles is interpreted in the strict sense of total energy calculation, the application to electrodes at the current stage of development is limited to computation of open circuit or rest voltages. Such calculations have however moved to the forefront of computational condensed matter science stimulated by a number of successful applications to electrocatalysis.[13–39] Electronic structure calculation in these studies is almost exclusively based on density functional theory (DFT) methods for extended systems. The standard approach to the modelling of extended systems is periodic replication of a finite supercell. The electrostatic boundary conditions in periodic models are artificial. As a result electronic energy levels must be aligned either with respect to vacuum or directly with respect to the standard hydrogen electrode. In this perspective we review two of the methods in use and illustrate this with the application to two popular model electrodes, the Pt(111)–water interface and the TiO_2(110)–water interface.

Electrochemists distinguish between two kinds of electrodes: reversible electrodes which are under the control of equilibrium exchange of charge with the electrolyte and electrodes which are not.[1–4] Electrodes showing near perfect reversible behaviour are also called ideally-non-polarizable. The voltage stays the same over a wide current window. In the opposite limit of vanishing charge transfer rates, the current is zero whatever the applied voltage until final breakdown occurs. Fermi levels in the electrode and electrolytic solution are not aligned. Only electrostatic forces are in equilibrium. The electrode acts as a capacitor admitting only current in response to varying voltage. A generic term often used for potentials of ideally polarizable electrodes is double layer potential even though reversible electrodes of course also develop electrical double layers. In this case, however, the interface potential is fixed by the chemical potential of reactants and products *via* Nernst law. Without this thermodynamic constraint, the double layer potential is critically dependent on the details of the structure of the double layer. This makes a huge difference for calculation.

The theory of double layers is an integral part of electrochemistry and has its foundations in the continuum theory of electrolytic solutions.[4,40,41] The Gouy–Chapman theory of the diffuse double layer is probably the best example. It is also one of the highlights of the development of theoretical physical chemistry. More recently the continuum approach has been supplemented with atomic force field modelling capable of treating compact layers[40,42–44] and ionic liquids.[41,45–48] The focus of most of this work is on the structure and capacitance of double layers. Classical modelling is however in general not suitable for the understanding of the potential of zero charge (PZC). This is the rest potential of an uncharged electrode.[49] The interaction with the aqueous solvent, however, can still lead to appreciable shifts in the energy levels of the electrode. This is where electronic structure calculation becomes inevitable. Another example is the effect of specific adsorption (chemisorption) which can also be viewed as a (partial) discharge. The first electronic structure theories of electrochemical interfaces were again based on continuum representations such as the jellium model of s,p metals.[49]

The best performing electrocatalysts are transition metals with active d electrons forming specific chemical bonds with surface species. This is the realm of surface science. The application of DFT based electronic structure calculation to heterogeneous catalysis is one of the success stories of computational science (see *e.g.* ref. 50). It was soon realized that the same methods can be applied to electrocatalysis at the metal–water interface with minimal changes.[13,20,21] Solvation and double layer potentials can be ignored in first approximation. This drastic simplification can be justified for key electrocatalytic reactions, such as hydrogen and oxygen evolution and the reverse hydrogen oxidation and oxygen reduction. The surface intermediates are fully discharged chemisorbed species similar to the charge neutral adsorbates at metal gas-phase interfaces. The difference is that the intermediates are created by exchange of electrons with the electrode and protons with the solution. However, if each oxidation is coupled to deprotonation and reduction to protonation the net reaction amounts to (de)hydrogenation and the free energy change can be obtained in first approximation using the proven methods of computational surface science. Electrode potential and pH can be accounted for by balancing the reaction free energies against fixed activity (mass) terms similar to the way partial pressure is treated in gas-phase thermochemistry or concentration in solution chemistry. This appealing and powerful DFT scheme has become most popular and numerous applications have appeared.[13–20] The same method has also been applied to catalysis by transition metal oxides,[21–26] even though, because of the ionic nature of these compounds, the exclusion of charged intermediates is questionable.

Electric double layer potentials have a profound effect on the rates of charge transfer between the metal and an ion holding on to a coordination shell of solvent molecules (outer sphere charge transfer). Modelling of electrified interfaces is therefore a challenge "first principle" computational electrochemistry will eventually have to face. Indeed, this has become a very active field and a variety of methods have been developed. One option is to adapt the implicit solvent methods of quantum chemistry.[51–53] Only water molecules in direct contact with the solid are included in the electronic structure calculation. The electrolytic solution further out is described by a continuum model.[18,25–33] The alternative is a fully explicit solvent approach.[16,34–39,54–66] This leads to a substantial increase in computational costs. Continuum models have several further advantages. They can describe diffuse double layers and the free energies of surface reactions can be compared to free energies of homogeneous reactions computed using the same implicit solvent model. However, this perspective will take a fundamentalistic view of "first principles" calculation and focus on explicit solvent methods only.

While reversible potentials can be calculated from reaction free energies, evaluation of PZC is a rather different problem. The PZC specifies the position of the Fermi level of an

electrode *before* electron exchange has aligned the Fermi level with an active redox couple. Or the solution may not contain any active redox couple at all. The PZC can thus be regarded as an intrinsic characteristic of an electrochemical interface. Level shifts due to interactions with aqueous solvent can be significant, even in the absence of net charge, and are dependent on the metal (see ref. 4 and references therein). However, computation of PZC is not only a matter of including solvent in the electronic structure calculation. The PZC must be represented on the same scale as used for the reversible potentials of redox reactions, which is by convention the standard hydrogen electrode (SHE). PZC computation is therefore inherently a question of level alignment.

Alignment schemes of electronic energy levels at electrochemical interfaces can be divided according to their choice of energy reference. As mentioned, the majority of methods have their roots in computational surface science. The energy reference in surface science is vacuum. The quantity calculated in the electrochemical extension of these methods is therefore the work function of a metal in contact with water. The work function is converted to the electrochemical scale by subtracting the absolute SHE potential.[34,35,37,38,55–57] The alternative is using some internal reference similar to electrochemical experiment. A convenient choice for internal reference is the free energy of a proton.[16,39,54,55,64–66] The energy levels computed in this approach are also in essence workfunctions. However, the electron is inserted (or removed) together with a proton in solution. The net effect is hydrogenation of the system. The short name we will use for this scheme is therefore the hydrogen insertion method although this is somewhat misleading because electrons and protons remain separated. These two methods can be seen in a common framework. Indeed, as we will show, both the work function and hydrogen insertion method can be derived from the modern theory of absolute electrode potentials.[4,67–72]

The configuration of the model system is a further distinction between methods with important implications for the computation of potentials. The model system can be a wet solid slab terminated by vacuum on both sides[16,37,38,54–57] or a two phase system of solid and water layers without vacuum.[34,35,39,64–66] Periodic boundary conditions are applied and the central difficulty is dealing with the effect on the electrostatics. In this respect there is a parallel with the computation of band-offsets at solid–solid heterojunctions and the question of the energies of charged impurities in semiconductors.[64] Resolving these issues for electrochemical interfaces is again closely linked to the definition of absolute electrode potentials.[55] We start this review therefore with a brief account of this challenging but for computational electrochemistry crucial subject. This will be the basis for a formal presentation of both the electron work function and hydrogen insertion method.

The work function method is the natural tool for metal electrodes. The same method can be used for metal-oxide electrodes. For this class of systems, however, the use of the hydrogen insertion method has distinct advantages. The reason is that transition metal oxides, in addition to being redox active, often also show acid–base activity.[73–76] Proton exchange with solution is not necessarily coupled to electron transfer and can occur independently in response to changes in pH of the electrolyte. The excess or missing proton charge is again compensated in a double layer. The position of electronic energy levels of metal oxides is therefore dependent on pH. A complete description of metal oxide electrodes must therefore also account for protonation and deprotonation of surface groups. Reversible protonation of a basic group in solution (a water molecule) is the key operation in the hydrogen insertion method and can be easily adapted for other aqueous species. Implemented consistently, the hydrogen insertion method therefore provides the unified framework for the treatment of redox properties and acidity required for the modelling of transition metal oxide water interfaces.[65,66,77]

Electronic structure calculation should ultimately help answering fundamental questions in physical electrochemistry such as where in the double layer the electron transfer takes place.[78] Methods for the computation of electrode potentials should therefore ideally be equally suitable for application to homogeneous redox reactions. This is also useful for the assessment of the catalytic effect of heterogeneous reactions which requires comparison to the uncatalyzed homogeneous reaction.[66] In previous publications we have shown that the hydrogen insertion method also meets this requirement.[79–81] In fact, the implementation of the hydrogen insertion method we have developed in ref. 80 and 81 has its origin in the free energy perturbation (FEP) schemes used in solution chemistry.[82,83] This in computational physical chemistry classical topic is also part of computational electrochemistry.

The perspective starts with a summary of the electrochemical concepts at the foundation of the calculation of electrode potentials. This is material found in most (but not all) textbooks on electrochemistry. After this preparation the key expressions used in the calculation of electrode potentials are presented and justified. This is the subject of Section 2. The next two sections are more technical discussions of how this formalism is applied in the workfunction method (Section 3) and in the hydrogen insertion method (Section 4). The question how electrode potential calculation and level alignment are interrelated is also discussed in Section 4. Section 5 reviews the FEP scheme for reversible insertion of electrons and protons used in the Density Functional Theory based Molecular Dynamics (DFTMD) implementation of the hydrogen insertion method developed by our group.

Theory and method are illustrated with two topical applications. The first is the calculation of the potential of zero charge of the Pt(111)–water interface. The second example is a calculation of the position of the band edges of the rutile TiO_2(110)–water interface relative to the standard hydrogen electrode. These two systems are benchmark models for metal and wide gap semiconductor electrodes, respectively, and the results we will present are taken from the literature. We also examine the band offsets between aqueous Pt and liquid water at pH 0 and TiO_2 and liquid water at the point of zero proton charge (pH 5) and compare to experiment. The density functional estimates for the absolute positions of valence and conduction band of water are new and presented in this publication for the first time.

A recurring issue in the discussion of energy levels in condensed phases is the accuracy of the DFT approximation.

As is well known, the workhorse in condensed phase calculations, the generalized gradient approximation (GGA),[84–86] has a rather mixed performance in band structure calculation.[87] The problem has become known as the delocalization error.[88–90] The magnitude of this error is non-uniform, depending on the degree of localization of the orbitals. As we will see, the alignment of the band edges of a metal (Pt), a semiconductor (TiO_2) and an insulator (H_2O) is very instructive for an assessment of the effect of the delocalization error on charge transfer at electrochemical interfaces. We will also compare to the results based on hybrid functionals.[91] These calculations have become feasible only recently thanks to advances in the implementation of exact exchange under periodic boundary conditions.[92]

2 Electrochemical background

The gap between what is measured in electrochemical experiment and what can be computed by electronic structure calculation appears at first discouragingly wide, more so than for example for spectroscopy. The questions are not only technical but also conceptual. Calculation of electrode potentials is a good illustration of this dilemma. What is needed first is a formal theory of electrode potentials linking these quantities to work functions. A key issue in this theory is the specification of a thermochemical standard state for the electron. This is also the crucial step in the definition of an absolute electrode potential accessible to experiment. This has led to some controversy among electrochemists which was in the end resolved by Trasatti.[67–69,71] The Trasatti scheme and the corresponding estimate of the absolute potential of the SHE (4.44 V) have now been generally adopted.[4,51–53,72] The theory he developed also provides the formal underpinning of the methods for computation of electrode potentials.[38,55] The summary of this theory presented in this section closely follows Fawcett[4,72] including the notation for multiphase systems.

2.1 Resolution of the electrochemical potential

The thermodynamic potential controlling electrochemical equilibrium is the electrochemical potential $\tilde{\mu}_i^\alpha$ defined for component i in phase α by

$$\tilde{\mu}_i^\alpha = \frac{\partial G^\alpha}{\partial n_i} \tag{1}$$

Here n_i is the quantity (mass) of component i in phase α with Gibbs free energy G^α. Electrochemical potentials are separated in a chemical and electrical contribution

$$\tilde{\mu}_i^\alpha = \mu_i^\alpha + q_i\phi^\alpha \tag{2}$$

μ_i^α is the chemical potential of component i in phase α, q_i its charge and ϕ^α is the inner potential of the phase also referred to as Galvani potential. The units we use are absolute microscopic units. This means that n_i in eqn (1) is the number of particles of species i and q_i in eqn (2) the charge of a single particle. The activity dependence of the chemical potential in these units is given by the expression

$$\mu_i^\alpha = \mu_i^{\alpha,o} + k_B T \ln a_i^\alpha \tag{3}$$

with a_i^α the activity of i in phase α. In ideal solutions $a_i^\alpha = \rho_i^\alpha/c^o$ where ρ_i^α is the number density and $c^o = 1$ mol dm^{-3} is the standard concentration. $\mu_i^{\alpha,o}$ is the corresponding standard chemical potential.

For eqn (1) and (2) to make sense the phase α must be finite and conducting. Only for finite bodies we can define the increase in free energy due to addition of macroscopic amounts of *charged* particles, as implied by eqn (1). Excess charge in conductors accumulates at the surface. The potential inside a conductor is constant and given by ϕ^α. The Galvani potential accounts therefore for charge imbalances at the surface only. These also include possible surface dipoles. To make this explicit the Galvani potential is further resolved in a surface dipole potential χ^α and the outer potential ψ^α.

$$\phi^\alpha = \psi^\alpha + \chi^\alpha \tag{4}$$

ψ^α, or Volta potential, is measured at a point in vacuum "just outside" the surface of phase α. This point is chosen close enough to the surface that (almost) all the work to bring a test charge from infinity towards a surface with a net charge density has been done but still at a sufficiently long distance away to be out of reach of image forces.[2] This is also the reference point for the work function W_i^α of a charged particle i specifying the reversible work needed to take it out of phase α.

The relation between chemical potentials and work functions is at the very heart of the theory of electrode potentials. The electrochemical potential $\tilde{\mu}_i^\alpha$ is the negative of the reversible work for transferring a particle from solution all the way to infinity. A separate potential is introduced for the work of bringing the particle to just outside the surface of a phase. This is the real potential defined as

$$\alpha_i^\alpha = \tilde{\mu}_i^\alpha - q_i\psi^\alpha = \mu_i^\alpha + q_i\chi^\alpha \tag{5}$$

The workfunction W_i^α is the difference between the standard real potential $\alpha_i^{\alpha,o}$ and the standard chemical potential $\mu_i^{g,o}$ of species i in the gas-phase[4]

$$W_i^\alpha = \mu_i^{g,o} - \alpha_i^{\alpha,o} \tag{6}$$

The work function should be distinguished from the solvation free energy

$$\Delta_s G_i^{\alpha,o} = \mu_i^{\alpha,o} - \mu_i^{g,o} \tag{7}$$

which is based on a comparison of chemical potentials. The difference is a change of sign and the contribution of the surface potential

$$\Delta_s G_i^{\alpha,o} = -(W_i^\alpha + q_i\chi^\alpha) \tag{8}$$

The solvation free energy is the negative of the workfunction for neutral solutes ($q_i = 0$), but not for ionic solutes.

After this preparation we are now ready to write down one of the central equations of this review, the expression for the real potential of the aqueous proton. Rearranging eqn (6) the standard real potential can be written as

$$\alpha_i^{\alpha,o} = -W_i^\alpha + \mu_i^{g,o} \tag{9}$$

The form of eqn (9) is familiar from the solution chemistry of neutral species. The chemical potential in solution is separated

in a contribution from solvation (the excess chemical potential) and a gas-phase term describing the chemical activity of the species.[93] The chemical reference state for hydrogen is the hydrogen molecule. $\mu_i^{g,o}$ in eqn (9) is therefore the free energy for the formation of a proton from H_2 in the gas-phase.

$$\tfrac{1}{2}H_2(g) \rightarrow H^+(g) + e^-(vac.) \qquad (10)$$

The standard free energy change of the reaction of eqn (10) can be computed from the free energy for dissociating a H_2 molecule in $H^\bullet$ atoms and the ionization potential of $H^\bullet$. Denoting this energy by $\Delta_f G^{g,o}_{H^+}$ and substituting in eqn (9) we have

$$\alpha^o_{H^+} = -W_{H^+} + \Delta_f G^{g,o}_{H^+} \qquad (11)$$

where we have suppressed the superindex for the aqueous phase. The first term is the solvation free energy of the proton (eqn (8)) corrected for the surface dipole effect. The value of $\Delta_f G^{g,o}_{H^+}$ at $T = 298$ K is given in the thermodynamic tables of gas-phase chemistry as 15.73 eV. However, in solution chemistry it is convenient to use the same reference for activity in solution and the gas-phase (see for example ref. 51). This makes the workfunction (eqn (6)) and solvation free energy (eqn (7)) independent of the definition of standard state. The gas phase activity is therefore represented relative to standard concentration and not standard pressure ($p^o = 1$ bar). At $T = 298$ K the difference, the so-called standard state compression term, $k_B T \ln(RTc^o/p^o) = 82$ meV. The ^{o} symbol is officially reserved for the pressure based reference of gas-phase chemistry. Rather than introducing yet another superscript we will stick with our unconventional notation at the risk of creating confusion. This means that $\Delta_f G^{g,o}_{H^+}$ will have to be adjusted to 15.81 eV. The discussion of the all important value of W_{H^+} will be deferred to Section 2.4.

We close this section with a reminder of a fundamental issue in electrochemistry: not all the quantities in eqn (1)–(6) are accessible to measurement by electrochemical or thermodynamic methods.[1–4] Only the electrochemical potential ($\tilde{\mu}_i^\alpha$), the work function (W_i^α) or equivalently the real potential (α_i^α) and the Volta potential (ψ_α) are. Eqn (2), (4) and (6) are therefore formal resolutions. It is not possible to assign actual values to the separate terms, the chemical potential (μ_i^α), the Galvani potential (ϕ^α), nor the surface potential (χ^α), without making "extra-thermodynamic" assumptions. These quantities must therefore be considered "unphysical", at least from the point of view of thermodynamics.[94] This statement, called the "Gibbs–Guggenheim principle" in ref. 94, is often met with disbelief from theoretical and computational chemists, in particularly in the case of the chemical potential (eqn (3)). The standard chemical potential $\mu_i^{\alpha,o}$ is in essence the solvation free energy $\Delta_s G_i^{\alpha,o}$ of species i. One would hope that a molecular simulation contains all information needed to compute $\Delta_s G_i^{\alpha,o}$. Indeed, there seems to be a way around this thermodynamic verdict for computation and also mass spectroscopy.[4,51–53,72,95] This continues to be, however, hazardous territory, in particular for DFT calculations in periodic systems.[96–98]

2.2 Interface and cell potentials

Electrochemical interfaces couple chemical to electrical energy. The interconversion is driven by gradients in Galvani potential between metal (or semiconductor) electrodes and the electrolytic solution. The special notation used in ref. 4 for the Galvani potential difference between a phase α (for example the electrolytic solution) and β (the metal) is

$$_\alpha\Delta_\beta\phi = \phi^\beta - \phi^\alpha \qquad (12)$$

A single Galvani (inner) potential difference is again not directly accessible to experiment because it always takes two electrodes to measure a voltage. What can be measured however is the difference $_\alpha\Delta_\beta\psi = \psi_\beta - \psi_\alpha$ between Volta (outer) potentials at a triple air–electrode–electrolyte interface (see Fig. 1). $_\alpha\Delta_\beta\phi$ and $_\alpha\Delta_\beta\psi$ are related to each other and the surface potentials χ_α and χ_β of the two phases (eqn (4)) by a loop taking the electron out of one phase and inserting it in the other phase as indicated in Fig. 1.

$$_\alpha\Delta_\beta\phi = {}_\alpha\Delta_\beta\psi + \chi^\beta - \chi^\alpha \qquad (13)$$

This relation will be needed in Section 2.3 for the definition of absolute electrode potentials.

Galvani potential differences play the role of components in an electrochemical circuit. In this review we will be only concerned with the open circuit voltage at zero current. Under these conditions the interface potentials add up to the cell potential U. This elementary model of an electrochemical cell was already proposed by Volta more than 200 years ago. We will apply this model to the reduction of a neutral free radical $X^\bullet$ to the anion X^- in aqueous solution. An example is the $OH^\bullet/OH^-$ couple. The electron is supplied by the oxidation of H_2. Using the generic notation of s for an electrolytic solution (aqueous solution in this case) and g for the gas-phase this reaction is written as

$$X^\bullet(s) + \tfrac{1}{2}H_2(g) \rightarrow X^-(s) + H^+(s) \qquad (14)$$

In the microscopic units adopted in Section 2.1 the standard reaction free energy $\Delta_r G^o$ is given as an energy per particle measured in units of eV. Dividing by the charge of an electron ($-e_0$) gives the standard SHE potential $U^o = -\Delta_r G^o/e_0$ of the $X^\bullet/X^-$ couple. Free radicals such as $OH^\bullet$ are highly reactive. Reaction (14) is therefore strongly exergonic and U^o is large

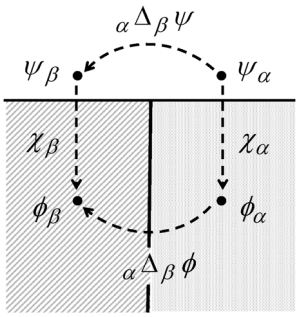

Fig. 1 Relation between the difference in Galvani potential ($\Delta\phi$) and Volta potential ($\Delta\psi$) at the triple electrode–electrolyte–air interface. Surface potentials (χ) are by definition positive when the potential increases entering a phase (hatched areas in figure).

and positive (U^{o} = 1.9 V for reduction of the aqueous hydroxyl radical[99]). Next we set up a cell with a rest potential equal to the free energy change of reaction (14). The following configuration meets our requirements

$$\mathrm{Cu|Pt,\ H_2(g)|HCl,\ H_2O||H_2O,\ NaX,\ X^{\bullet}|M|Cu'} \quad (15)$$

The product anion (X^-) and cation (H^+) are neutralized by Na^+ and Cl^- coions, respectively. The double vertical lines stand for a salt bridge which has been inserted to separate the acidic anode solution from a cathode solution of higher pH. For the anode metal we have chosen Pt. This metal is the most effective catalyst for hydrogen oxidation. The material of the cathode is left as an unspecified metal M because it will be important for our argument that the cathode and the anode are not made from the same metal. On the other hand it is crucial that the voltmeter is connected to electrodes of identical composition, which is why the two Cu terminals were added. This ensures that the full Fermi level difference between electrodes is available to carry out electrical work. We note that the cell 15 is hypothetical for $OH^{\bullet}$ because the redox potential of this and other aggressive free radicals[99] is outside the stability window of the aqueous solvent.

The potential U of an electrochemical cell is by definition the potential difference between the electrode on the right hand side (as written) with respect to the one on the left hand side. For the cell 15 we have therefore $U = {}_{\mathrm{Cu}}\Delta_{\mathrm{Cu}'}\phi$ in the notation of eqn (12). Going around a circuit, potential differences should add up to zero (Volta's law). The open circuit potential of cell 15 can therefore be written as

$$U = {}_{\mathrm{Cu}}\Delta_{\mathrm{Pt}}\phi + {}_{\mathrm{Pt}}\Delta_{\mathrm{S}}\phi + {}_{\mathrm{S}}\Delta_{\mathrm{M}}\phi + {}_{\mathrm{M}}\Delta_{\mathrm{Cu}'}\phi \quad (16)$$

where the aqueous solvent is indicated by S. Eqn (16) holds provided that the electrical contact over the salt bridge has cancelled any potential difference between the electrolytic solutions in the cathode and anode compartments. Electrodes and copper leads attached to them are always in equilibrium and we can equate the electrochemical potentials $\tilde{\mu}_e$ for the electrons. Setting $\tilde{\mu}_e^{\mathrm{Pt}} = \tilde{\mu}_e^{\mathrm{Cu}}$ we find for the first term in eqn (16)

$${}_{\mathrm{Cu}}\Delta_{\mathrm{Pt}}\phi = \frac{1}{e_0}(\mu_e^{\mathrm{Pt,o}} - \mu_e^{\mathrm{Cu,o}}) \quad (17)$$

where $\mu_e^{m,o}$ is the intrinsic chemical potential of an electron in metal m. Eqn (17) follows from eqn (3) recalling that activities of electrons in metals are unity. The same procedure can be applied to the M–Cu′ contact. Substituting in eqn (16) and rearranging terms gives

$$U = \left({}_{\mathrm{S}}\Delta_{\mathrm{M}}\phi - \frac{\mu_e^{\mathrm{M,o}}}{e_0}\right) - \left({}_{\mathrm{S}}\Delta_{\mathrm{Pt}}\phi - \frac{\mu_e^{\mathrm{Pt,o}}}{e_0}\right) \quad (18)$$

Expression (18) for the open circuit (also called rest) potential of cell 15 is completely general making no assumptions about reversibility of the electrode reactions. Even if the rate of the cathode or anode reaction of cell eqn (15) is very slow, prohibiting electron exchange, eqn (18) will still hold. In fact, eqn (18) is valid for all cells with electrodes made out of Pt and M metal (see ref. 4). The left electrode of cell 15 is however an hydrogen electrode which serves as a reference electrode and is therefore in equilibrium. The Galvani potential at the Pt interface is fixed by the H^+ and H_2 activities and can be found from the Nernst equation for the half reactions (see also eqn (2) and (3)). The activity of H^+ is effectively its concentration $[H^+]$. The activity of H_2 is measured by its partial pressure p_{H_2}. This gives for the Pt|S interface

$$e_0\,{}_{\mathrm{S}}\Delta_{\mathrm{Pt}}\phi = \mu_{H^+}^{o} + \mu_e^{\mathrm{Pt,o}} - \frac{1}{2}\mu_{H_2}^{o} + k_B T \ln\frac{[H^+]}{c^o}\sqrt{\frac{p^o}{p_{H_2}}} \quad (19)$$

where we have suppressed the superscript S specifying the aqueous phase for H^+ and g for H_2. Setting activities of H^+ and H_2 to unity and inserting in eqn (18) we obtain

$$U_{\mathrm{M|S}}(\mathrm{she}) = \left({}_{\mathrm{S}}\Delta_{\mathrm{M}}\phi - \frac{\mu_e^{\mathrm{M,o}}}{e_0}\right) - \left(\frac{\mu_{H^+}^{o} - \frac{1}{2}\mu_{H_2}^{o}}{e_0}\right) \quad (20)$$

Eqn (20) is an expression for the potential of the M|S electrode relative to the SHE. To make this explicit for later reference the notation of U has been extended accordingly. As expected the dependence on the Fermi level of Pt has cancelled out.

Imposing also equilibrium on the $X^{\bullet}(S) + e^-(M) \rightarrow X^-(S)$ half reaction at the right hand electrode we recover the Nernst equation for the potential of cell 15

$$U_{X^{\bullet}/X^-}(\mathrm{she}) = -\frac{1}{e_0}\left(\mu_{X^-}^{o} + \mu_{H^+}^{o} - \mu_{X^{\bullet}}^{o} - \frac{1}{2}\mu_{H_2}^{o} + k_B T \ln\frac{a_{X^-}}{a_{X^{\bullet}}}\right) \quad (21)$$

The quantity in brackets on the right hand side of eqn (21) is the free energy change of the cell reaction eqn (14) (under standard conditions for the hydrogen electrode). The standard potential *vs.* SHE for $X^{\bullet}/X^-$ reduction, in our notation denoted by $U_{X^{\bullet}/X^-}^{o}(\mathrm{she})$, is obtained for unit activity of the $X^{\bullet}$ radical and X^- anion.

2.3 Absolute electrode potentials and work functions

In introductory textbooks the cell equation (eqn (21) for our system) is derived by equating chemical and electrical work. What the much more elaborate derivation of Section 2.2 gains us is that it can be generalized into a definition of absolute electrode potential.[68] This definition is valid for all electrodes, reversible or not. Applied to eqn (20) the argument goes as follows (our presentation again relies on ref. 4). The solvent in the cell specified by eqn (15) is water. Adding the surface potential of water denoted by χ^{S} to the terms inside each of the brackets of eqn (20) separates U in two potentials

$$U_{\mathrm{M|S}}(\mathrm{she}) = U_{\mathrm{M|S}}(\mathrm{abs}) - U_{H^+/H_2}^{o}(\mathrm{abs}) \quad (22)$$

which are given by

$$U_{\mathrm{M|S}}(\mathrm{abs}) = {}_{\mathrm{S}}\Delta_{\mathrm{M}}\phi - \frac{\mu^{\mathrm{M,o}}}{e_0} + \chi^{\mathrm{S}} \quad (23)$$

$$U_{H^+/H_2}^{o}(\mathrm{abs}) = \frac{\mu_{H^+}^{o} - \frac{1}{2}\mu_{H_2}^{g,o}}{e_0} + \chi^{\mathrm{S}} \quad (24)$$

The potentials of eqn (23) and (24) depend on properties of one electrode only and can be regarded as single electrode potentials. A similar claim could already be made for the quantities between brackets in eqn (18). The potentials of eqn (23) and (24), however, are workfunctions and can be

interpreted as absolute electrode potentials as anticipated by the notation. This is why the surface potential was added in. With this additional term we can replace $\mu^{o}_{H^+}$ by the real potential $\alpha^{o}_{H^+}$ combining eqn (24) with eqn (5).

$$e_0 U^{o}_{H^+/H_2}(\text{abs}) = \alpha^{o}_{H^+} - \frac{1}{2}\mu^{g,o}_{H_2} \qquad (25)$$

In Section 2.1 we have already derived an expression for the real potential of the aqueous proton. This is eqn (11). This involved choosing a reference state for the proton for which we took the regular reference state for hydrogen in the gas-phase, namely molecular hydrogen. To be consistent we must set therefore $\mu^{g,o}_{H_2} = 0$ in eqn (25). Then with eqn (11) for the real potential, eqn (25) leads to

$$e_0 U^{o}_{H^+/H_2}(\text{abs}) = \Delta_f G^{g,o}_{H^+} - W_{H^+} \qquad (26)$$

As explained in ref. 4 ion work functions are uniquely defined thermochemical constants that can be measured using electrochemical cells with air gaps. Both terms in eqn (26) are therefore known from experiment (see further Section 2.4).

Eqn (23) should be valid when the M|S electrode is under control of an equilibrium redox couple such as in cell 15. ${}_S\Delta_M\phi$ is now again determined by the Nernst equation for the $X^{\bullet}(S) + e^-(M) \rightarrow X^-(S)$ half reaction and we find

$$\begin{aligned} e_0 U_{M|S}(\text{abs}) &= e_0 U_{X^{\bullet}/X^-}(\text{abs}) \\ &= \alpha^{o}_{X^{\bullet}} - \alpha^{o}_{X^-} + k_B T \ln \frac{a_{X^{\bullet}}}{a_{X^-}} \end{aligned} \qquad (27)$$

The difference in real potentials can be expanded using eqn (9)

$$\alpha^{o}_{X^{\bullet}} - \alpha^{o}_{X^-} = \mu^{g,o}_{X^{\bullet}} - \mu^{g,o}_{X^-} + W_{X^-} - W_{X^{\bullet}} \qquad (28)$$

The right hand side of eqn (28) represents a thermodynamic cycle consisting of desolvating the anion X^-, ionizing it in the gas-phase and reinserting the product radical $X^{\bullet}$ in solution. This is the definition of the adiabatic ionization potential (AIP) of an aqueous species. However, instead of removing the electron all the way to infinity, it is left at the reference point used for workfunctions. With this electrochemical definition of ionization the absolute standard potential for the $X^{\bullet}/X^-$ couple is according to eqn (27) simply equal to the AIP.

$$U^{o}_{X^{\bullet}/X^-}(\text{abs}) = \frac{\text{AIP}_{X^-}}{e_0} \qquad (29)$$

Substitution in eqn (22) using eqn (26) gives U *vs.* SHE

$$e_0\, U^{o}_{X^{\bullet}/X^-}(\text{she}) = \text{AIP}_{X^-} + W_{H^+} - \Delta_f G^{g,o}_{H^+} \qquad (30)$$

The first term AIP_{X^-} can be regarded as an electronic workfunction specifying the work needed to extract an electron bound in X^-. Comparing eqn (30) to eqn (21), we see that the standard reaction free energy has been reinterpreted in terms of workfunctions, which is what will enable us to compare $U^{o}_{X^{\bullet}/X^-}$ to the energies measured in photo emission spectroscopy (PES).

What if the M|S interface is ideally polarizable inhibiting charge transfer between metal and solution? Can expression eqn (23) for the absolute electrode potential again be transformed to a sum of ionization energies or workfunctions? The answer is yes. This can be achieved by substituting eqn (13) with α = S and β = M. The dependence on the solvent surface potential χ^S in eqn (23) is eliminated in favour of χ^M, the surface potential of the metal. χ^M, in turn, can be combined with $\mu^{M,o}_e$ to the work function W^M_e of an electron in metal M. The result is the expression for absolute electrode potential proposed in ref. 68 in its most general form.

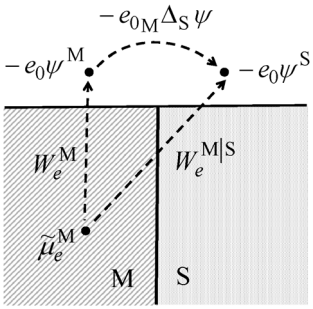

Fig. 2 Diagram visualising eqn (32). W^M_e is the reversible work for transferring an electron from inside metal M to a point in vacuum just outside the metal surface. $-e_{0M}\Delta_S\psi$ is the work for moving it from there to a point just outside the solution S. The sum $W^{M|S}_e$ defines the absolute electrode potential of the M|S interface.

$$U_{M|S}(\text{abs}) = \frac{W^M_e}{e_0} + {}_S\Delta_M\psi \qquad (31)$$

W^M_e in eqn (31) can be determined by photo emission spectroscopy or thermionic emission. The Volta potential step ("contact potential") is also accessible to experiment. It can be measured using a Kelvin probe.[4] Moreover, also this quantity can be represented as work: $-e_{0M}\Delta_S\psi$ is the energy required to carry an electron through vacuum from a point just outside the metal to a point just outside the solution (see Fig. 2). Rewriting eqn (31) accordingly

$$e_0 U_{M|S}(\text{abs}) = W^M_e - e_{0M}\Delta_S\psi \equiv W^{M|S}_e \qquad (32)$$

suggests that $W^{M|S}_e$ can be interpreted as the minimum energy required to extract an electron from the metal and deliver it to the vacuum region on the water side. As we will see in Section 3, $W^{M|S}_e$ can be calculated using the methods of computational surface science. The potential *vs.* SHE is obtained by substituting in eqn (22)

$$e_0 U_{M|S}(\text{she}) = W^{M|S}_e - U^{o}_{H^+/H_2}(\text{abs}) \qquad (33)$$

2.4 Experimental estimate of the absolute SHE

A key constraint for the definition of the absolute hydrogen electrode potential in Section 2.3 was that it can be determined by experiment.[68,69] Eqn (26) relates $U^{o}_{H^+/H_2}(\text{abs})$ to the workfunction of the proton. This is not the only possibility. Consider a mercury electrode at the point of zero charge. Mercury electrodes are the textbook example of an (almost) ideally polarizable electrode. Rearranging eqn (22) we can write

$$U^{o}_{H^+/H_2}(\text{abs}) = U^{pzc}_{Hg|S}(\text{abs}) - U^{pzc}_{Hg|S}(\text{she}) \qquad (34)$$

Table 1 Summary of the experimental data for the determination of the absolute standard hydrogen electrode potential according to eqn (26) and (35). All data except the last two rows have been taken from Table 1 of Trasatti's 1986 "explanatory note".[68] Also listed is his recommended value for the absolute SHE. The value for the solvation free energy is from ref. 95. The estimate for the surface potential has been obtained using eqn (8)

$\frac{1}{2}H_2(g) \rightarrow H^+(g) + e^-(vac.)$	$\Delta_f G^{g,o}_{H^+} = 15.81$ eV
Work function of $H^+(aq)$	$W_{H^+} = 11.36$ eV
Potential of zero charge of Hg	$U^{pzc}_{Hg\|S}$ (she) $= -0.191$ V
Electron workfunction of Hg	$W^{Hg}_e = 4.50$ eV
Volta potential difference	$_S\Delta_{Hg}\psi = -0.248$ V
Recommended value for absolute SHE[68]	$U^o_{H^+/H_2}$(abs) $= 4.44$ V
Solvation free energy of $H^+(aq)$[95]	$\Delta_s G^o_{H^+} = -11.53$ eV
Surface potential of water (from eqn (8))	$\chi^S = +0.17$ V

Standard state for H^+ is the ideal gas at 1 mol dm^{-3}.
Standard state for e^- is vacuum at rest.

Substituting eqn (31) yields

$$U^o_{H^+/H_2}(\text{abs}) = \frac{W^{Hg}_e}{e_0} + {}_S\Delta_{Hg}\psi - U^{pzc}_{Hg|S}(\text{she}) \qquad (35)$$

Surveying the experimental data needed as input for eqn (26) and (35) available at the time Trasatti decided that $U^o_{H^+/H_2}$(abs) $= 4.44$ V is the best estimate.[68] This value was accepted by IUPAC as their recommended value. Fawcett[72] has recently reviewed the procedure taking into account also experimental data from mass spectroscopy experiments.[95] His conclusion was that only a small adjustment was necessary (from 4.44 V to 4.42 V). The experimental input data for estimating the absolute hydrogen electrode potential are crucial parameters for the link between electrochemistry, spectroscopy and computation. We have therefore reproduced Table 1 of ref. 68 in Table 1.

The mass spectroscopy data of ref. 95 are of special interest because what is measured by this technique is the chemical potential $\mu^o_{H^+}$ rather than real potential $\alpha^o_{H^+}$ (from a formal perspective this statement has the status of an "extra-thermodynamic" assumption[4,51–53]). Recall from eqn (5) that $\alpha^o_{H^+}$ and $\mu^o_{H^+}$ are related to each other by the surface potential χ^S of water. A similar relation holds for the solvation free energy and the workfunction (eqn (8)). Applying this relation to the experimental estimates in Table 1 yields $\chi^S = 170$ meV as listed in the last row of the table. This indirect estimate is consistent within 50 meV with estimates of χ^S from other sources.[72] It should be mentioned that there are good arguments that 4.44 V is not the appropriate value for use in quantum chemistry calculations.[51–53] For the conversion of redox potentials computed using implicit solvent models a value of $U^o_{H^+/H_2}$(abs) based on the chemical potential rather than the real potential is more consistent (see also ref. 72).

3 Electron work function method

3.1 Model system

Workfunctions are referred to vacuum. The slab geometry familiar from computational surface science is the natural system setup for this purpose. The slab is terminated on both sides by surfaces in contact with vacuum. To turn this into a model of an electrochemical interface, one of the surfaces is covered with a layer of water. A schematic example is shown in Fig. 3. Solid slab plus water layer are periodically replicated in the x and y direction with the z-axis perpendicular to the slab. The simplest approach is to apply also periodic boundary conditions in the z direction separating the periodic images by a sufficiently wide vacuum buffer to eliminate short range interactions. Long range interactions of systems without net charge can be cancelled by inserting a sheet of dipoles in the vacuum between slab images.[100,101] To extend this scheme to electrified interfaces the metal slab is charged. The excess charge on the metal surface is compensated either by real ions (protons) in the water layer[16,54] or by a fictitional counter electrode.[34,35,37,38] For details we refer to the original literature.

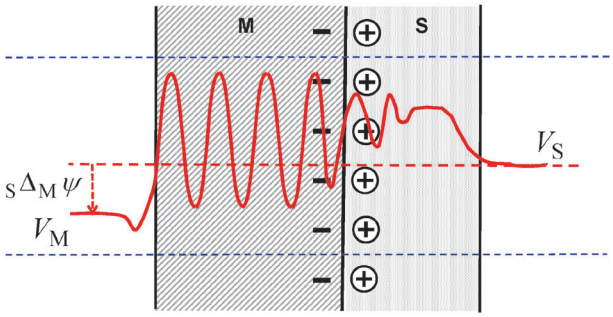

Fig. 3 The vacuum–electrode–electrolyte–vacuum model system used in workfunction methods. The metal (M) has a net negative charge compensated in a double layer by the positive charge in the solution (S). The thin dashed lines mark the periodically repeated supercell. The curve is a schematic representation of the electrostatic potential. The difference in asymptotic potentials on the M and S side gives the contact potential.[38]

The workfunction of the metal is estimated from the position of the Fermi level relative to the asymptotic value of the potential in vacuum. If we use the potential plateau on the *metal* side of the model, indicated by V_M in Fig. 3, we should obtain the workfunction W^M_e of the bare metal. What is the result if we had used instead the asymptotic value V_S on the *solvent* side? Comparing Fig. 3 to Fig. 2 we conclude that this should give an estimate of $W^{M|S}_e$ of eqn (32) from which we obtain the potential of the interface using eqn (33). Two different workfunctions for the same system may appear a paradox at first because there is only one Fermi level. However, for metal–water slabs carrying a net dipole in the z direction $V_S \neq V_M$. This is a peculiarity of the periodic boundary conditions in the x, y dimensions and distinguishes extended slab models from cluster models. Consistent with this, $-e_0(V_S - V_M)$ is the work to move the electron from the metal to the water side making up for the difference between $W^{M|S}_e$ and W^M_e. For a metal–solution–air interface (see Fig. 1) this work is given by $-e_{0M}\Delta_S\psi$ which is equal to the second term in eqn (32). Summarizing these relations we can write

$$V_M - V_S = {}_S\Delta_M\psi = \frac{W^{M|S}_e - W^M_e}{e_0} \qquad (36)$$

The conclusion is that despite appearances, the slab geometry of Fig. 3 is a faithful model of an electrode immersed in water.

This argument, as far as we are aware, was first pointed out by Otani *et al.* in ref. 38.

3.2 Potential of zero charge of Pt(111)

The workfunction method is the workhorse of computational electrochemistry. Here we review only the application to a particularly sensitive quantity, the potential of zero charge of a platinum electrode. Platinum is one of the best performing electrode materials for fuel and electrolysis cells. Still the energy loss due to overpotentials is significant even for Pt electrodes.[15,29] This is the motivation for the numerous computational studies of Pt electrodes that have appeared and continue to appear. The Pt(111)–water interface is therefore also the obvious candidate for computation of the potential of zero charge. Pt electrodes are however not easy systems for experimental determination of the PZC because of the proximity to the threshold for underpotential deposition of hydrogen. After a survey of the literature Jinnouchi and Anderson in ref. 28 decided on a PZC of 0.4 V *vs.* SHE as a good mean value. Here we will follow their recommendation and will use this value to assess the accuracy of computational estimates of the Pt PZC listed in Table 2. References to the experimental literature are not given here but can be found in ref. 28. Table 2 (row a) also gives the experimental value for the workfunction of the bare metal (again as quoted in ref. 28) and the decrease as a result of the interaction with water. Note that the shift for the Pt electrode (−1.1 eV) is significantly larger than the −0.25 eV for the Hg electrode given in Table 1.

All computational estimates of the PZC in Table 2 have been obtained using the work function method summarized in Section 3.1. The main difference is the representation of the solvent. The treatment of the solvent is crucial because, as observed by several authors,[28,55,57] changes in the orientation of the water molecules can bias $U^{pzc}_{Pt|S}$ up or down by a full Volt. Proper averaging of these large fluctuations requires in principle sampling of the thermal motion of the solvent using molecular simulation methods. This is how the results of Otani *et al.*[38] (row b) and Schnur and Gross[57] (row e) were obtained. Both calculations are averages over a first principle molecular dynamics (MD) trajectory. The water layer in simulation b was sufficiently thick (≈11 Å) to approach bulk conditions away from the surface. The water model in calculation e was much smaller consisting only of a single water bilayer. To avoid the high computational costs of MD sampling Tripkovic *et al.*[55] developed a set of criteria for selecting minimal representative static structures of the water layer. Their prediction for the PZC is listed in rows c and d. Computational costs can be further reduced by combining explicit water molecules with a dielectric continuum model of the solvent. Calculations using this approach were pioneered by Jinnouchi and Anderson.[28] Some of their results are listed in rows f and g.

Table 2 Estimates of the potential of zero charge (PZC) *vs.* SHE of a Pt(111) electrode ($U^{pzc}_{Pt|S}$ in the notation of Section 2.3) computed using a variety of models for the water layer (ML = monolayer, BL = bilayer, see the text of Section 3.2 for further explanation). W^{Pt}_e is the workfunction of the bare Pt(111) surface (units eV). $\Delta W^{Pt}_e = W^{Pt|S}_e - W^{Pt}_e = e_{0S}\Delta_M\psi$ is the shift in the work function induced by the interaction with water (see eqn (36)). The experimental PZC estimate of 0.4 V is the value recommended by ref. 28 on the basis of a survey of the literature

	DFT	Solvent	W^{Pt}_e	ΔW^{Pt}_e	$U^{pzc}_{Pt\|S}$	Ref.
a	Experiment		5.93	−1.1	0.4	28
b	PBE	11 Å(MD)	5.8	−1.2	0.2	38
c	PBE	2BL(static)	5.74	−1.09	0.21	55
d	RPBE	2BL(static)	5.60	−0.14	1.02	55
e	PBE	1BL(MD)	—	−0.7	0.6	57
f	RPBE	Cont.	5.96	−0.39	1.13	28
g	RPBE	0.5 ML + cont.	5.96	−1.1	0.5	28

For an evaluation of the results in Table 2 we first note that all calculations are effectively in agreement on the value for the work function of the bare metal. The DFT estimate is moreover close to experiment confirming that Fermi levels of metals in the generalized gradient approximation end up at the right energy relative to vacuum as has been verified in numerous computational studies of metal vacuum interfaces. The data in Table 2 seem to indicate that the same is true for the Pt surface in contact with water provided that a sufficiently realistic model of the water layer is used. Without any explicit water the solvent effect is underestimated as can be seen from the PZC in row f. This effect is explained in ref. 28 in terms of competition between electronic and configurational contributions which can only be accounted for by adding a sufficient number of explicit adsorbed water molecules. Of some concern is the disappointing performance of RPBE in the calculation of row d. Comparing to row c suggests that the PZC shows an increased sensitivity to details of the GGA functional. This is however somewhat puzzling in view of the good track record of RPBE in heterogeneous catalysis studies. We also note that ref. 28, which is the source of the results of row f and g, makes no mention about discrepancies between the RPBE and PBE.

4 Hydrogen insertion method

4.1 Oxidation and reduction of electrodes

The idea behind the hydrogen insertion method is to mimic the hydrogen electrode. Addition of an electron to the electrode is coupled to insertion of a proton in solution. The free energy for this operation should be a direct estimate of the potential of the electrode *vs.* SHE. Conversion to or from absolute potentials is not necessary. While this scheme may appear intuitively correct, a formal justification is not entirely straightforward just as was the case for the work function method. One of the problems is that it is not obvious how to relate insertion free energies to cell potentials without the help of Nernst law. Recall that cell potentials were formally defined in Section 2.2 in terms of Galvani potential differences. The point of this fundamental definition (eqn (16)) was that it did not yet distinguish between reversible electrodes and polarizable electrodes not under control of a redox couple. Also the proton insertion method should be completely general in this respect. In this section we will clarify this question by deriving the hydrogen insertion method from the theory of the absolute electrode potentials summarized in Section 2.3.

The hydrogen insertion method is based on the resemblance of eqn (33) to a equation for the free energy of a chemical reaction.

To turn this into a practical scheme for calculation we first substitute eqn (26) for the absolute hydrogen electrode potential

$$e_0 U_{\mathrm{M|S}}(\mathrm{she}) = W_{\mathrm{e}}^{\mathrm{M|S}} + W_{\mathrm{H^+}} - \Delta_{\mathrm{f}} G_{\mathrm{H^+}}^{\mathrm{g,o}} \qquad (37)$$

$W_{\mathrm{e}}^{\mathrm{M|S}}$ was equated in Section 2.3 to the (minimum) work to transfer an electron from inside the metal to a point just outside the solution (see also Fig. 2). Comparing to eqn (30) for the potential of the $\mathrm{X^\bullet/X^-}$ couple we see that the adiabatic ionization potential $\mathrm{AIP_{X^-}}$ plays a similar role. The last two terms in eqn (37) and (30) concern the hydrogen reference electrode and are the same. This parallel suggests that eqn (37) can be interpreted as the free energy change of the reaction

$$\mathrm{M} + \mathrm{H^+(s)} \rightarrow \mathrm{M^+} + \tfrac{1}{2}\mathrm{H_2(g)} \qquad (38)$$

where M represents the electrode. If we rename the work-function $W_{\mathrm{e}}^{\mathrm{M|S}}$ to an adiabatic ionization potential $\mathrm{AIP_M}$, eqn (37) assumes a form identical to eqn (30) with the metal M as the electron donating species instead of the anion $\mathrm{X^-}$. So we can write

$$e_0 U_{\mathrm{M^+|M}}(\mathrm{she}) = \mathrm{AIP_M} + W_{\mathrm{H^+}} - \Delta_{\mathrm{f}} G_{\mathrm{H^+}}^{\mathrm{g,o}} \qquad (39)$$

Pushing the analogy between electrodes and aqueous solutes the reference to the solvent in the subscript of U has been dropped. The subscript is now a label for the redox couple of reaction (38).

Reaction eqn (38) is not equivalent to reaction (14) in every respect. Reactants and products of eqn (14) have zero net charge while the total charge in reaction (38) is $+1e_0$. The origin of the net positive charge is the uncompensated proton which serves as the reference electrode for the oxidation. However, the free energy of reaction (38) can also be computed if we take the proton from a water molecule. This transforms the reaction from a charge transfer to a charge separation

$$\mathrm{M} + \mathrm{H_2O} \rightarrow \mathrm{M^+} + \mathrm{OH^-} + \tfrac{1}{2}\mathrm{H_2(g)} \qquad (40)$$

Reaction (40) is more convenient for DFTMD simulation because it takes place in a charge neutral system. Coupling to the recombination of the aqueous proton and the hydroxide anion

$$\mathrm{H^+(s)} + \mathrm{OH^-} \rightarrow \mathrm{H_2O} \qquad (41)$$

recovers reaction (38). The free energy change of the coupled process is found by adding the contributions of each step

$$e_0 U_{\mathrm{M^+|M}}(\mathrm{she}) = \mathrm{AIP_M} + \mathrm{ADP_{H_2O}} - 2.30\, k_{\mathrm{B}} T \mathrm{p}K_{\mathrm{W}} - \Delta_{\mathrm{f}} G_{\mathrm{H^+}}^{\mathrm{g,o}} \qquad (42)$$

where $\mathrm{ADP_{H_2O}}$ is the adiabatic deprotonation energy of a water molecule in solution. $\mathrm{p}K_{\mathrm{W}}$ is the dissociation constant of water. The electrode potentials of eqn (42) and (40) are indeed identical because of the Brønsted relation between the work function of a solvated proton ($W_{\mathrm{H^+}}$) and a proton bound in a $\mathrm{H_2O}$ molecule ($\mathrm{ADP_{H_2O}}$)

$$\mathrm{ADP_{H_2O}} = W_{\mathrm{H^+}} + 2.30 k_{\mathrm{B}} T \mathrm{p}K_{\mathrm{W}} \qquad (43)$$

Eqn (43) will be discussed in more detail in Section 5.2 where the application of the hydrogen insertion method to the computation of acidity constants is reviewed.

Instead of oxidizing M we could consider reducing M. Coupled to oxidation of hydrogen the reduction is described by the cell reaction

$$\mathrm{M} + \tfrac{1}{2}\mathrm{H_2}(g) \rightarrow \mathrm{M^-} + \mathrm{H^+(s)} \qquad (44)$$

Represented as an electrode potential the free energy change of reaction (44) is written as

$$e_0 U_{\mathrm{M|M^-}}(\mathrm{she}) = \mathrm{AEA_M} + W_{\mathrm{H^+}} - \Delta_{\mathrm{f}} G_{\mathrm{H^+}}^{\mathrm{g,o}} \qquad (45)$$

where AEA is the adiabatic electron affinity. We have now two expressions for the electrode potential of a metal, $U_{\mathrm{M^+|M}}$ of eqn (39) or equivalently eqn (42) and $U_{\mathrm{M|M^-}}$ of eqn (45). How do these potentials compare and which one is the one measured in experiment? The energy for removing an electron from the Fermi level of a metal is the same as is gained by adding it. Either eqn (42) or (45) can be used to compute the electrode potential. In contrast, for molecules the oxidation states $\mathrm{X^+}$, X and $\mathrm{X^-}$ are different chemical species and in general $U_{\mathrm{X^+/X}} > U_{\mathrm{X/X^-}}$. Semiconductors are more complicated than either metals or molecules. Electrode potentials for semiconductors will be discussed at the end of the next section.

4.2 Adiabatic and vertical levels

The electrode potentials in Section 4.1 are derived from adiabatic ionization potentials or electron work functions. For solids the electron workfunction can be determined in thermionic emission experiments. In photo emission experiments the atomic configuration is given no time to relax and the ionization energies measured by PES methods are vertical ionization potentials. The vertical IP of a solid gives, after a change of sign, the position of the valence band maximum (VBM). The vertical attachment energy (electron affinity), which in some cases can be measured by inverse PES, probes the states at the conduction band minimum (CBM). The formalism we have developed can be equally applied to align these vertical energy levels with respect to the SHE. The expression for the VBM on the SHE scale is found by replacing the adiabatic IP in eqn (39) with the vertical IP

$$e_0 U_{\mathrm{VBM}}(\mathrm{she}) = \mathrm{IP_M} + W_{\mathrm{H^+}} - \Delta_{\mathrm{f}} G_{\mathrm{H^+}}^{\mathrm{g,o}} \qquad (46)$$

where $\mathrm{IP_M}$ stands for the vertical ionization potential of M. Similarly modifying eqn (45), we can position the CBM relative to the SHE

$$e_0 U_{\mathrm{CBM}}(\mathrm{she}) = \mathrm{EA_M} + W_{\mathrm{H^+}} - \Delta_{\mathrm{f}} G_{\mathrm{H^+}}^{\mathrm{g,o}} \qquad (47)$$

where EA is the vertical electron affinity.

The potentials U_{VBM} and U_{CBM} defined in eqn (46) and (47) are energy levels represented as potentials *vs.* SHE, not electrode potentials that can be measured as open circuit potentials of electrochemical cells. The electrode potential is determined by the Fermi level. This distinction is crucial for semiconductors. There is (in equilibrium) only one Fermi level. $W_{\mathrm{e}}^{\mathrm{M}}$ is the reversible work for addition or removal of electrons. The same applies to the interface workfunction $W_{\mathrm{e}}^{\mathrm{M|S}}$ which differs from $W_{\mathrm{e}}^{\mathrm{M}}$ with respect to the reference point in vacuum (see Fig. 2). However, the Fermi level is not an electronic state which can give up or accept electrons. It is an thermodynamic energy level. Of course, this is in principle also true for metals,

but for metals (minus) the vertical IP in the groundstate is a good approximation for the Fermi level. So is the negative of the vertical EA electron affinity. This doesn't work for semiconductors. The Fermi level is located somewhere in between the VBM and CBM where the density of states is zero. The Fermi level of semiconductors is not directly accessible for DFTMD simulation with fixed numbers of electrons. What can be computed are the vertical IP and EA using eqn (46) and (47). The potential of the semiconductor electrode must be computed from U_{VBM} and U_{CBM} using the appropriate expression for the Fermi level which also contains the conduction electron and valence band hole densities and their effective masses.

4.3 Model systems. Full *versus* half reaction scheme

The hydrogen insertion method as it is understood here is an all-atom scheme treating all of the system at the same level of theory. The geometry of the model system is obviously a critical issue in this approach. In the scheme proposed by Rossmeisl *et al.*[16,54,55] reaction (38) (or rather the reverse) takes place in a slab geometry similar to Fig. 3 retaining the two interfaces with vacuum. In ref. 39, 65 and 66 the vacuum buffer has been eliminated. Protons and electrons are inserted in a system consisting of periodically repeated slabs of solid and layers of solvent as depicted in Fig. 4. This geometry is similar to the models of heterojunctions in solid state physics.[102,103]

Comparing Fig. 4 to 3 we immediately notice a major complication for methods that rely on model systems of the type of Fig. 4. While the mean electrostatic potential in the solid and liquid subsystems can be specified unambiguously with respect to vacuum in Fig. 3, in the absence of a vacuum layer it is not clear what the electrostatic reference is in Fig. 4. This reference is in general unknown. It is also unphysical as has been recognized in computational solid state physics at an early stage.[104] The conventional Ewald summation method for the evaluation of electrostatic interactions in periodic systems introduces shifts in the zero of the potential anywhere between 1 eV and 10 eV.[65,80,81,96–98] This is why coupled insertion of an electron and proton pair is necessary. Electrons and protons are inserted or removed simultaneously. The free energy for the coupled removal is the sum of the adiabatic ionization potential and proton workfunction in eqn (30) and (39) (or equivalently eqn (42) and (45)). The net charge of the system is conserved. Any constants added to the electrostatic potential cancel (notice that experimental electrochemistry faces a very similar problem[4]). The uncertainty in the reference of the electrostatic potential must be clearly distinguished from finite system size effects which of course are also a source of error.

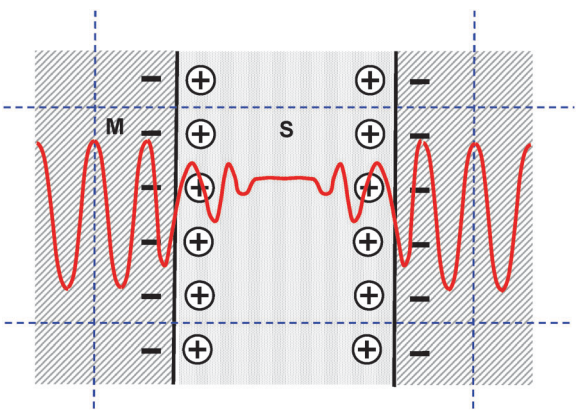

Fig. 4 Metal(M)–solvent(S) model system used in the hydrogen insertion method. Full 3D periodic boundary conditions are applied without insertion of vacuum separators. The supercell, indicated by the thin dashed lines, contains two separate solid–water interfaces, one for each side of the slab. Double layers are modelled by solid slabs and liquid layers of opposite charge (*cf.* Fig. 3). The net dipole moment of the cell is zero on average. The curve is an example of an electrostatic potential in this geometry.

The coupled insertion scheme described above is the most direct (and safe) implementation of the hydrogen insertion method. It will be referred to as the full reaction scheme to distinguish it from a half reaction scheme. In the half reaction scheme protons and electrons are inserted sequentially. The model system can be the same but electrons and protons can also be added to different systems. This is the mode in which the hydrogen insertion method is applied in the calculation of redox potentials of species in homogeneous solution, such as the aqueous organic molecules studied in ref. 80 and 81. The ionization of these molecules was carried out in a regular cubic MD cell containing the molecule and the solvent. The work function of the proton was computed by reversible insertion of a proton in a MD cell of similar size without the redox active solute. The condition for such a half reaction scheme to work is that the electrostatic reference in the two cells is the same. If not, the bias due to the periodic boundary conditions will not cancel out. We will return to the issue in more detail in Section 5.

An application leaving us no other option than using a half reaction scheme is the calculation of the effective potentials of the VBM and CBM. As explained in Section 4.2, what is needed in eqn (46) and (47) are vertical energies for removal or addition of electrons. Coupled insertion of electrons and protons, however, delivers the reversible ionization potential with the solvation free energy of the proton as reference. To obtain the vertical IP relative to the same reference, we must compute the energy for vertical removal of an electron separately from the free energy for adiabatic removal of the proton and then substitute the results in eqn (46) to obtain U_{VBM}. A similar procedure with vertical addition instead of removal of the electron yields an estimate of U_{CBM} using eqn (47).

4.4 Coupling acid–base and redox reactions

The hydrogen insertion method enables us to compute electrode potentials and free energy changes of homogeneous reactions at the same level of theory. A class of reactions for which such a unified treatment is vital are acid–base reactions. This was demonstrated in our study of the thermochemistry of deprotonation coupled oxidation of three well-known model redox active organic molecules in bulk solution (hydrobenzoquinone,[80] tyrosine and tryptophan[81]). The link between redox and acid base chemistry is best visualized by the proton coupled electron

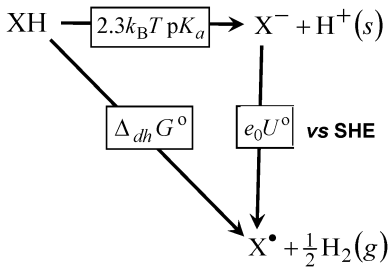

Fig. 5 Relation between the dehydrogenation free $\Delta_{dh}G^o$ energy of a hydride XH, its pK_a and the standard reduction potential U^o of the conjugate base X^-.

transfer (PCET) triangle familiar from physical organic chemistry.[105] The triangle for an hydride XH is given in Fig. 5. X can be a molecule (ion) or solid surface.[66,77,106,107]

Starting with the acid dissociation (horizontal arrow in Fig. 5)

$$XH(s) \rightarrow X^-(s) + H^+(s) \qquad (48)$$

and then transferring an electron form the conjugate base (X^-) to the aqueous proton (vertical arrow)

$$X^-(s) + H^+(s) \rightarrow X^\bullet(s) + \tfrac{1}{2}H_2(g) \qquad (49)$$

should give the same product as direct dehydrogenation of XH (reaction along the diagonal arrow)

$$XH(s) \rightarrow X^\bullet(s) + \tfrac{1}{2}H_2(g) \qquad (50)$$

The free energy of solvation of the proton is the common reference for the equilibrium constant of both reaction (48) and (49). The reverse of reaction (49) is reaction (14) defining the redox potential of X^- *vs.* SHE. Expressing the equilibrium constant of reaction (48) in terms of the pK_a of XH, Hess law is satisfied if

$$\Delta_{dh}G^o_{XH} = 2.30\,k_BT\,pK_{aXH} + e_0U^o_{X^\bullet/X^-}(\text{she}) \qquad (51)$$

where $\Delta_{dh}G^o_{XH}$ is the standard free energy change of reaction (50).

5 Free energy perturbation method

The hydrogen insertion method for the computation of electrode potentials is in essence a free energy perturbation (FEP) method. The free energy that is computed is the reversible work for inserting particles in a condensed phase system. The method we use is a DFTMD implementation[108] of Warshel's microscopic version[82,83] of Marcus theory of electron transfer.[109] Recently this scheme has been generalized to reversible insertion of protons for the calculation of pK_a.[110] The method has been presented in detail in ref. 80 and 81. Here we summarize the expressions used in calculations and refer to the two technical papers just mentioned for explanation.

5.1 Thermodynamic integration

Free energies in electronic structure calculation are computed from total energy differences. The scheme used in our approach to convert total energy differences into a free energy difference is based on thermodynamic integration of energy gaps. Reactants R are transformed into products P using an auxiliary (mapping) Hamiltonian $\mathscr{H}_\eta$ which is a linear combination of the Hamiltonian for the reactants and that for the products, $\mathscr{H}_\eta = (1-\eta)\mathscr{H}_R + \eta\mathscr{H}_P$. Here η is a coupling parameter which is gradually increased from 0 (reactants) to 1 (products). Intermediate values $0 < \eta < 1$ correspond to hybrid systems that are a mixture of R and P. These systems have no physical counterpart in experiment, but may be simulated by determining the atomic forces from the corresponding Hamiltonian $\mathscr{H}_\eta$. Canonical averages over MD configurations obtained with Hamiltonian $\mathscr{H}_\eta$ will be denoted by brackets $\langle\cdots\rangle_\eta$. The total free energy change ΔA is calculated from the integral of the vertical energy gap ΔE with respect to the coupling parameter:

$$\Delta A = A(\eta=1) - A(\eta=0) = \int_0^1 d\eta \langle \Delta E\rangle_\eta \qquad (52)$$

The gap ΔE is defined as the potential energy difference between initial and final configurations, from which an electron e^-, a proton H^+, or both, have been removed, while keeping all other atoms fixed.

The coupling parameter integral eqn (52) converts vertical energy gaps (ΔE) into adiabatic gaps (ΔA). How this works is best illustrated for the example used previously, the reduction of a neutral radical $X^\bullet$ to the anion X^- (reaction 14). However, as explained in Section 4.1 the same procedure is applied for computation of the potential of a metal electrode. The particle that is removed is an electron. Conform the notation of ref. 80 and 81, the vertical energy gap between the oxidized and reduced state (solute plus solvent) will be indicated by $\Delta_{ox}E_{X^-}$ with the subscript specifying the solute. Eqn (52) gives the corresponding adiabatic energy gap

$$\Delta_{ox}A_{X^-} = \int_0^1 d\eta \langle \Delta_{ox}E_{X^-}\rangle_\eta \qquad (53)$$

The integrand at the reactant end, $\langle\Delta_{ox}E_{X^-}\rangle_{\eta=0}$, is the vertical IP of X^- averaged over the thermal fluctuations of the solvent. Vertical electron detachment energies of anions can measured in Photo Emission Experiments which are now also feasible for electrolytic solutions.[111,112] The average gap $\langle\Delta_{ox}E_{X^-}\rangle_{\eta=0}$ computed by the DFTMD simulation would be equal to the experimental IP, for the exact functional, if it were not for the complication mentioned at the end of Section 4.3, namely the uncertainty in the reference for electrostatic potentials in systems under periodic boundary conditions. The bias V_0 in the reference for DFTMD potentials as a result of this uncertainty was discussed in some detail in ref. 80 and 81. It acts as an offset $-e_0V_0$

$$\langle\Delta_{ox}E\rangle_{\eta=0} = IP_{X^-} - e_0V_0 \qquad (54)$$

where IP_{X^-} now stands for the true unbiased IP for a given functional. For stable condensed phase systems $V_0 > 0$. Removing electrons from periodic model system costs less energy than from the same system with a interface to vacuum.

The gap at the product end $\langle\Delta_{ox}E\rangle_{\eta=1}$ of the integral eqn (53) is a similarly biased estimate of the vertical electron

affinity (electron attachment energy) $EA_{X^\bullet}$ of the oxidation product, the radical $X^\bullet$.

$$\langle \Delta_{ox} E \rangle_{\eta=1} = EA_{X^\bullet} - e_0 V_0 \quad (55)$$

Thermodynamic integration interpolates between these two extremes. In the limit of linear solvent response this amounts simply to taking the mean value[82,83,108]

$$\Delta_{ox} A_{X^-} = \frac{1}{2}(IP_{X^-} + EA_{X^\bullet}) - e_0 V_0 \quad (56)$$

In the non-linear generalization of eqn (56) the $\frac{1}{2}$(IP + EA) term is replaced by the adiabatic ionization potential (AIP) introduced in eqn (29) and we can write

$$AIP_{X^-} = \Delta_{ox} A_{X^-} + e_0 V_0 \quad (57)$$

with $\Delta_{ox} A_{X^-}$ given by eqn (53).

The AIP is directly the absolute electrode potential of a redox couple (eqn (29)). Unfortunately, as mentioned in Section 4.3 it is not possible to use eqn (57) because V_0 is in general not known. The point of the hydrogen insertion method is that we don't need to know V_0 for computation of the electrode potential relative to the SHE because the workfunction of the proton in periodic systems is also biased by V_0, but with the opposite sign. The challenge is therefore to find a procedure for insertion/removal of a proton based on eqn (52) consistent with the FEP scheme for electron removal. This procedure should be equally suitable for the computation of acidity constants and was in fact originally developed for that purpose.[110] In the next section we therefore will review first the proton insertion method for computation of pK_a.

5.2 Acidity constants

Computation of potentials of mean force is the natural domain for application of FEP methods. The potential of mean force describes the effective interactions between solvated species. Also the equilibrium constant of a dissociation reaction in solution can be derived from the potential of mean force. This approach has also been employed for computation of acidity constants.[113,114] However, as explained in Section 4.4, coupling to redox reactions poses rather strict constraints on the treatment of acid–base reactions. Consistency with a computational hydrogen electrode forces us to base also the computation of acidity on the insertion of protons. This can be achieved by a thermodynamic cycle transferring the acid proton from the acid to the point just outside the solution and reinserting it again as a solvated proton. Such a scheme was proposed in ref. 110 and worked out in detail in ref. 80 and 81. The pK_a of the acid dissociation reaction $XH \rightarrow X^- + H^+$ is obtained from the following expression

$$2.30\, k_B T\, pK_{aXH} = ADP_{XH} - W_{H^+} + k_B T \ln[c^o \Lambda_{H^+}^3] \quad (58)$$

The first term, ADP_{XH}, is the adiabatic deprotonation energy with the point just outside the solution interface as reference, W_{H^+} is again the workfunction of the aqueous proton. The last term accounts for the translational free energy generated by the dissociation.[81] This contribution has been approximated by the chemical potential of a free gas phase proton at standard concentration (c^o). Λ_{H^+} is the thermal wavelength of the proton. This approximation is justified because of the small mass of the proton compared to the conjugate base X^-. Under ambient conditions the translational contribution amounts to a correction of $k_B T \ln[c^o \Lambda_{H^+}^3] = -0.19$ eV or -3.2 eV units.

The deprotonation free energy is estimated from a thermodynamic integral eqn (52) (compare to the oxidation integral eqn (53))

$$\Delta_{dp} A_{XH} = \int_0^1 d\eta \langle \Delta_{dp} E_{XH} \rangle_\eta \quad (59)$$

where the energy gap in the integrand now corresponds to the energy for vertical deprotonation of XH. The adiabatic deprotonation energy ADP_{XH} of eqn (58) is obtained from $\Delta_{dp} A_{XH}$ of eqn (59) according to[81]

$$ADP_{XH} = \Delta_{dp} A_{XH} - e_0 V_0 - \Delta_{zp} E_{H(X)} \quad (60)$$

Eqn (60) is similar to eqn (57). However, the bias due to the shift in the electrostatic reference appears with the opposite sign because the particle that is removed has a positive charge. We have also added a zero point motion correction. This is necessary because the DFTMD simulation as it is usually applied treats all nuclei as classical particles. The approach adopted in ref. 81 is to subtract the zero point energy of the acid proton attached to the base in full solution. All other protons are classical particles. This effective acid proton zero point motion is indicated by $\Delta_{zp} E_{H(X)}$ in eqn (60). $\Delta_{zp} E_{H(X)}$ is estimated from the peaks in the (classical) velocity autocorrelation function of the acid proton as obtained from the DFTMD trajectory.

Vertical detachment or attachment of protons is not feasible in experiment. Still, we can calculate the vertical deprotonation energy $\Delta_{dp} E$ in eqn (59), by switching off the charge of the acid proton, transforming it in a "dummy". Applied to XH this process can be viewed as the fictitious discharge reaction $XH \rightarrow Xd^-$ where d is a dummy proton. While d has no Coulombic interactions with the electrons and nuclei in the system, it is subject to a harmonic restraining potential V_{restr} keeping it close to the equilibrium position of the H^+ nucleus in the protonated system. This construction ensures that the deprotonation is reversible. Letting the system relax and switching the charge of the dummy back on, we obtain the protonation energy corresponding to inserting a proton in the position defined by the dummy. The reasons why this procedure can be carried out in practice are special to the geometry of hydrogen bonds.[80,110] Perturbations by a properly tuned restraining potential are minimal but can still have some effect on the deprotonation free energy. An approximate analytic expression for these perturbations has been worked out in the appendix of ref. 81. It is shown there that provided minimum and spring constants of the restraining potential are matched to the geometry and vibrational frequencies of the acid proton, the error is small compared to other sources of uncertainty in the calculation. Corrections for the restraining potential have therefore been ignored in eqn (60).

The expression for pK of eqn (58) also contains the workfunction W_{H^+} of the proton. Computation of W_{H^+} is the key

step in our proton insertion scheme. It is estimated by the deprotonation free energy of the hydronium cation (H_3O^+). The H_3O^+ ion is modelled by a (flexible) pyramidal structure stabilized by the restraining potential. Thus, identifying W_{H^+} with $ADP_{H_3O^+}$ we apply eqn (60) and find

$$W_{H^+} = \Delta_{dp}A_{H_3O^+} - e_0V_0 - \Delta_{zp}E_{H^+(OH_2)} \quad (61)$$

However the hydronium ion is not a regular acid. The classical trigonal H_3O^+ geometry on which our estimate for the work-function (solvation free energy) is based is only one of the configurations the solvated proton can adopt. The implications of this restriction are quantified below and discussed in detail in ref. 81. Substituting eqn (60) and (61) in eqn (58). we obtain for the pK of XH

$$2.30\, k_BT\, pK_{aXH} = \Delta_{dp}A_{XH} - \Delta_{dp}A_{H_3O^+} + k_BT\ln[c^oA^3_{H^+}] - (\Delta_{zp}E_{H(X)} - \Delta_{zp}E_{H^+(OH_2)}) \quad (62)$$

Assuming that differences in zero point motion of hydronium and acid can be ignored, the pK_a is the difference in deprotonation free energies adjusted by a constant. The constant, −3.2 units, is effectively the pK_a of the constrained hydronium ion, because in this case the deprotonation integrals and zero point motion terms rigorously cancel. The model H_3O^+ is therefore 1.5 K more acid than the pK_a = −1.74 of the hydronium in Brønsted theory.

The "zero-order" approximation to pK_a of eqn (62) was applied in ref. 81 to a test set of common small acids (CH_3OH, HCl, H_2S, CH_3SH, NH_4^+). The mean absolute deviation from experiment was 1 pK unit. All of the five acids were too basic. The systematic error is comparable to the error in the pK_a of the hydronium ion but is of opposite sign (see above). The dissociation constant of water was found to be underestimated by 2 pK units (see Section 6). This test seems to suggest that the accuracy of the calculation of pK_a in our all-atom DFT scheme is between 1 and 2 pK units (≈100 meV). All these calculations were carried out in a periodic cubic box of length 9.86 Å. Under ambient conditions such a box contains 32 water molecules. This is a rather small system. Moreover, in one of the protonation states the net charge of the cell is not neutral. Finite size errors in such a system can be expected to be significant. Electrostatic interactions in DFTMD are evaluated using an Ewald method. Net charge of a MD cell is compensated by a neutralizing background. The interaction between an ion, its images and the neutralizing background (The Wigner potential) is screened by polarization induced in the solvent. As it turns out, in a MD cell of cubic symmetry this leads to an almost perfect cancellation of errors.[115]

There is a further potential source of error related to system geometry. The calculation of the acidity of the test set of small acids was carried out applying what we have called in Section 4.3 a half reaction scheme. The deprotonation free energies for the acid and of the hydronium ion (eqn (59)) were determined in separate MD cells. For an unbiased estimate of pK, the V_0 offset potential in eqn 60 must be identical to the V_0 in eqn (61). V_0 is strongly dependent on the system composition. The model systems used in the small acid calculation consist almost completely of solvent. The variation in V_0 due to substituting one acid species by another or an hydronium ion is small. This condition was however more critical for the larger acid molecules we have investigated, which include an hydroquinone[80] and a number of amino acids.[81,116] In order to accommodate a molecule of this size 5 to 10 H_2O molecules will have to be removed and a cell of given dimensions will contain significantly less solvent than the same cell with only an hydronium molecule. Changes in V_0 can no longer be ignored and add to the error in the pK.[81] This complication is avoided when acid and hydronium share the same MD cell. Therefore, the full reaction scheme is preferred for systems with a solid/liquid interface. This is how the computation of the surface acidity of titania,[77] silica[106,107] and alumina[106] was performed. Also the computation of the potential of the aqueous TiO_2 electrode of ref. 65 and 66 used a full reaction scheme.

5.3 Redox potentials

Redox potentials are computed using eqn (30). The electronic and proton workfunctions are determined by evaluating the thermodynamic integrals for adiabatic oxidation of X^- (eqn (53)) and reversible deprotonation of the hydronium ion (eqn (59) with XH = H_3O^+). Substitution of eqn (57) and (61) in eqn (30) gives

$$e_0U^o_{X^\bullet/X^-}(\text{she}) = \Delta_{ox}A_{X^-} + \Delta_{dp}A_{H_3O^+} - \Delta_fG^{g,o}_{H^+} - \Delta_{zp}E_{H^+(OH_2)} \quad (63)$$

In contrast to the expression for pK_a (eqn (62)) the zero point motion term in the workfunction of the proton (eqn (61)) is not cancelled out. The value we use for $\Delta_{zp}E_{H^+(OH_2)}$ is 0.35 eV. This is a rough estimate which we determined by summing the zero point motion of three vibrational modes with frequencies obtained from the stretching, bending and librational peaks in the classical velocity auto correlation function of a proton in liquid water. A correction of −0.35 V amounts to a substantial decrease in reduction potential. Because it is inherent to the work function of the proton, the same quantum correction must be applied to potentials of interfaces when represented against the SHE. The $\Delta_fG^{g,o}_{H^+}$ term in eqn (63) is given the experimental value (15.81 eV) of Table 1.

To complete the free energy triangle of Fig. 5 we need an equivalent expression for the dehydrogenation free energy $\Delta_{dh}G^o_{XH}$ of XH, *i.e.* the free energy of reaction (50). If we don't want to rely on Hess law (eqn (51)) we can obtain an independent estimate by simultaneously removing a proton and an electron. In the notation we have introduced, the corresponding thermodynamic integral is written as

$$\Delta_{dh}A_{XH} = \int_0^1 d\eta\langle\Delta_{dh}E_{XH}\rangle_\eta \quad (64)$$

The vertical energy gap $\Delta_{dh}E_{XH}$ is the difference in total of energy of $X^\bullet$ (product) relative to XH (reactant) with the energy of the solvent included. Because the net charge of the systems remains the same, a bias in the electrostatic reference is of no concern. We must however again account for the free energy for the creation of three more translational degrees of freedom as well as the zero point motion energy of the acid

proton adding corrections similar to eqn 58 and 60, respectively. The result is that

$$\Delta_{dh}G^{o}_{XH} = \Delta_{dh}A_{XH} - \Delta_{f}G^{g,o}_{H^+} - \Delta_{zp}E_{H(X)} + k_B T \ln[c^{o}\Lambda^{3}_{H^+}] \quad (65)$$

The combined effect of the last two terms in eqn (65) is a downward adjustment of 0.54 eV, which is definitely not negligible. This correction is the sum of the corrections terms in eqn (62) for the pK and eqn (63) for the redox potential. Because the thermodynamic corrections add up, Hess law (eqn (51)) requires that the thermodynamic integrals satisfy the triangle relation of Fig. 5

$$\Delta_{dh}A_{XH} = \Delta_{dp}A_{XH} + \Delta_{ox}A_{X^-} \quad (66)$$

Eqn (66) is a most powerful condition to assess the statistical accuracy of the DFTMD sampling. The experience of the applications to date shows that the dehydrogenation free energy matches the free energy of sequential deprotonation and oxidation within an uncertainty of 100 meV for simulation runs of a duration accessible to DFTMD ($\approx$10 ps).

6 The uncatalyzed dehydrogenation of water

Abstraction of an hydrogen atom from a water molecule in bulk solution is probably the most fundamental reaction in electrochemistry and is therefore a benchmark for the validation of computational methods. It is the first and highest hurdle in the four electron oxidation of water to molecular oxygen and hydrogen. We use this reaction to illustrate the application of the all-atom DFTMD method. The results for the free energies were first reported in ref. 66. They are summarized in Table 3. The DFTMD model system was the familiar periodic cubic cell of length 9.86 Å containing 32 water molecules corresponding to ambient density. The DFTMD simulation was carried out using the CP2K package.[117,118] Technical details of the electronic structure calculation (basis sets, *etc.*) can be found in the original papers.[66,81] The table lists the thermodynamic integrals $\Delta_{ox}A$ of eqn (53), $\Delta_{dp}A$ of eqn (59) and $\Delta_{dh}A$ of eqn (64) and the reaction free energies ΔG derived from these integrals using eqn (62), (63) and (65) (differences in zero point corrections have been ignored). ΔA for oxidation and dehydrogenation was determined from the vertical energy gaps of five to six different values of the coupling parameter, each averaged over DFTMD trajectories of 5 to 10 ps. For deprotonation only 3 integration points were used (η = 0.0, 0.5, 1.0) but the runs were considerably longer (40 to 60 ps for BLYP).

Table 3 Standard free energy changes for the dehydrogenation of a water molecule in bulk solution (energies in eV). Thermodynamic integrals (eqn (52)) are denoted by ΔA, the reaction free energies calculated using these integrals by ΔG. BLYP and HSE06 results were taken from ref. 66. Experimental redox energies are from ref. 99. The data in the last row are the deprotonation integral and acidity of the hydronium ion (see Section 5.2 and ref. 81)

	BLYP		HSE06		
	ΔA	ΔG	ΔA	ΔG	Exp.
$H_2O \rightarrow OH^- + H^+$	16.34	0.7	16.29	0.7	0.83
$OH^- + H^+ \rightarrow OH^\bullet + \frac{1}{2}H_2$	2.10	1.3	2.52	1.7	1.9
$H_2O \rightarrow OH^\bullet + \frac{1}{2}H_2$	18.54	2.1	18.89	2.5	2.72
$H_3O^+ \rightarrow H_2O + H^+$	15.35	0.19	15.29	0.19	0.10

The standard state for H_2O is the liquid. Conversion of the acidity constant of H_2O to pK units yields therefore the pK_W. This is the convention used in Table 3. In practice this amounts to decreasing the free energies for deprotonation and dehydrogenation by a further $k_B T\log([H_2O]/c^o)$ = 104 meV. This energy, equivalent to −1.74 pK units, is by definition the Brønsted acidity of the hydronium. Both the BLYP and HSE06 calculations gave pK_W = 12, two pK units less than the experimental value of 14. The error in the oxidation free energies is significantly larger. Redox potentials are underestimated in the BLYP[84,85] approximation by as much as 0.6 V. The exact exchange component in the HSE06[91] functional reduces the error, but the redox free energies are still too low. Similar discrepancies were found in ref. 80 and 81. As explained there, we are confident that the error can be attributed to shortcomings in the DFT functional and not to finite system size or periodic boundary effects. Limitations in the system size could affect the free energy for the oxidation of the OH^- anion (a charge recombination). However, the dehydrogenation reaction (the diagonal in Fig. 5) which involves only neutral species suffers from the same problem. We will return to this issue in the conclusion at the end of the paper.

The last entry in Table 3 gives $\Delta_{dp}A_{H_3O^+}$, the integral for deprotonation of the constrained hydronium used in the calculation of the work function of the proton. The value of this quantity, which is central in the hydrogen insertion method, was taken from ref. 81. Recall that according to eqn (62) the pK_a of H_3O^+ is a constant whatever $\Delta_{dp}A_{H_3O^+}$ happens to be. Of course the work function of the proton depends on $\Delta_{dp}A_{H_3O^+}$ as is clear from eqn (61). Unfortunately the unknown bias in the electrostatic reference (V_0) makes it impossible to determine W_{H^+}. However, we can turn the argument around, and estimate V_0 by comparing to experiment.[80] The relevant data are gathered in Table 1, According to eqn (61) we should compare to the workfunction. This gives V_0 = 3.64 V. It is however not obvious whether the workfunction or solvation free energy is the more appropriate for this purpose. In ref. 80 we opted for the solvation free energy $\Delta_s G^o_{H^+}$ as determined in ref. 95. This would lead to V_0 = 3.47 V. Either value is in good agreement with the V_0 = 3.6 V obtained by Leung[97] using a non-empirical approach. These numbers are however somewhat larger than the 3.1 V computed in ref. 98 for a model of an actual water vacuum interface. We stress again that the value of V_0 is irrelevant for the calculation of the acidity and redox energies.

7 Alignment of the band edges of liquid water

7.1 Overview of experimental data

From an electronic structure perspective water can be regarded as a disordered wide gap insulator.[119] The fundamental gap as given in ref. 119 is 8.7 eV. This value has become the consensus experimental reference for computational work on the electronic structure of liquid water.[120–122] The position of the VBM can be estimated from the photo emission threshold of liquid water.

The measurements of the Winter–Faubel group give 9.9 eV below vacuum.[111,112] Adding the bandgap places the CBM at −1.2 eV relative to vacuum. It should be mentioned that the position and even definition of the CBM are the subject of some debate.[119,123] Coe *et al.* in ref. 123 argue in favour of a CBM at −0.5 V. Spectroscopic levels are referred to the SHE by adding the absolute SHE potential. The value we use is the 4.44 V of Table 1. Using the nomenclature introduced in Section 4.2 this gives U_{VBM}(she) = 5.5 V and U_{CBM}(she) = −3.2 V (see also Table 4). On the electrochemical scale these are extreme potentials which implies that electrochemical activation of liquid water is not easy.

7.2 Computation using hydrogen insertion

The methodology of Section 4.2 should enable us to align the DFT band edges of liquid water with the SHE. For a solid a single point calculation for the equilibrium geometry would be adequate for this purpose. For water, because of the liquid nature, averaging over thermal fluctuations is necessary. Ionization energies were sampled from a DFTMD trajectory of the same cubic 32 molecule system as used for the calculation of the single molecule free energies of Table 3. The calculation was however less demanding. Fluctuations in the energy gap for the pure liquid are small compared to the fluctuations in the energy gaps of solutes. The result for the time averages can be found in the first row of Table 4. The electrochemical equivalent of the VBM was obtained in a half reaction scheme as outlined in Section 4.3. The vertical ionization potential of the liquid (IP_{H_2O}) was substituted in eqn (46) together with the proton work function estimated according to eqn (61) from the $\Delta_{dp}A_{H_3O^+}$ given in Table 3.

Alternatively we could have used the average energy of the highest occupied molecular orbital (HOMO) of the liquid as an estimate of the VBM. This for chemistry crucial energy level will be indicated by ε_{HOMO}. The expression for aligning ε_{HOMO} to the SHE is again eqn (46) with the negative of the orbital energy instead of the IP. The results are also listed in Table 4. Effective potentials for band edges obtained from total energy differences and from orbital energies are sorted in separate columns labelled ΔE, respectively, ε. For the CBM we have only calculated the estimate based on orbital energies, obtained by replacing the vertical electron affinity in eqn (47) by minus the average energy (ε_{LUMO}) of the lowest unoccupied molecular orbital (LUMO).

The generalized gradient approximation (GGA) is notorious for underestimating bandgaps in solids. The discrepancy becomes worse for larger bandgaps.[87] The results for liquid water in Table 4 are in line with this expectation. The Kohn–Sham bandgap ($\varepsilon_{LUMO} - \varepsilon_{HOMO}$) in the BLYP approximation is 4.6 eV too small, consistent with what has been observed in previous investigations.[120–122] However our method also predicts absolute positions of band edges. What this additional information reveals is that the underestimation of the band gap is predominantly caused by a failure to account for the energies of the occupied orbitals. The effective potential of the HOMO is 3.5 V less positive, which places the VBM 3.5 eV above the VBM obtained from photo emission spectroscopy. The error in positioning the LUMO, 1 eV below the CBM in experiment, is comparatively smaller. Application of HSE06 raises the LUMO to about the correct level. Also the HOMO level improves. It moves to more positive potentials but not as much as is needed. The difference with experiment is still 2 V.

A related issue is the question of the equivalence between IP's computed form total energy differences (ΔSCF) and Kohn–Sham eigenvalues. For isolated molecules it is well known that the absolute value of ε_{HOMO} can be several eV less than the ΔSCF IP using the same GGA functional. These two quantities should be the identical in exact DFT.[124] Could this be the reason for the unrealistically high position of the HOMO in the GGA? The results in Table 4 suggest that this is not the case. The gap between ε_{HOMO} and −IP as computed for BLYP is 0.3 eV, which is only just above the statistical accuracy of the calculation (≈0.1 eV). For HSE06 the agreement is even better. A possible explanation for this for a chemist perhaps somewhat surprising observation can be found in ref. 88. There it is shown that for perfectly ordered solids ε_{HOMO} must be equal to −IP because of the extended nature of the orbitals in energy bands. This remains true even if the value is wrong. Our calculations suggest therefore that the behaviour of liquid water is closer to that of a solid than that of a molecule. We note in this context that the experimental IP of liquid water (9.9 eV) is 2.7 eV smaller than the IP of a gas-phase water molecule (12.6 eV, as quoted in ref. 124), which gives an indication of the band dispersion in liquid water.

Table 4 Valence band maximum (VBM) and conduction band minimum (CBM) of pure liquid water and the interface of water with Pt(111)(pH 0) and rutile TiO_2(110) (pH 5) represented as potentials *vs.* SHE in V. The vacuum level (vac.) is obtained by adding the IP of the dry surface to the VBM of the aqueous system. The potentials in the column labeled ΔE have been computed from total energy differences (vertical or adiabatic, see the text). Estimates computed from orbital energies are listed under the heading ε. The GGA (PBE) results for Pt(111) have been taken from ref. 38 (see Table 2). The table contains calculations for TiO_2(110) in two hydration states, a fully solvated interface (TiO_2(aq)) and covered with 1 ML of water ((TiO_2(1 ML)). The solid slabs consisted of 3 O–Ti–O layers (3 L) and 5 O–Ti–O layers (5 L). The results for the 3 L system are from ref. 65 and for the 5 L system from ref. 66. For the source of the experimental estimates for liquid water see Section 7.1. The experimental data for the Pt electrode are discussed in Section 3.2, and for TiO_2(110) in Section 9.1

		GGA		HSE06		
		ΔE	ε	ΔE	ε	Exp.
H_2O	VBM	2.31	1.97	3.65	3.56	5.5
	CBM		−2.60		−3.24	−3.2
	vac.	−4.44	−4.44	−4.44	−4.44	−4.44
Pt	Fermi		0.2			0.4
	vac.		−5.6			−5.5
TiO_2(aq)	VBM(3 L)	1.60	1.46			2.65
	CBM(3 L)	−0.42	−0.34			−0.35
	vac.(3 L)		−5.89			−5.8
	VBM(5 L)	1.28				,,
	CBM(5 L)	−0.27				,,
TiO_2(1 ML)	VBM(3 L)		1.62			,,
	CBM(3 L)		−0.14			,,
	vac.(3 L)		−5.73			,,
	VBM(5 L)		1.45		2.70	,,
	CBM(5 L)		−0.44		−0.66	,,
	vac.(5 L)		−5.65		−5.90	,,

The pathological character of the GGA treatment of the VBM of liquid water becomes even more clear when one tries to compute the adiabatic ionization potential. This is the third variant of the calculation of electrode potentials involving the evaluation of the adiabatic IP in a full reaction scheme (see Section 4.3) and substituting in eqn (39). We tried this for BLYP and found that it made little difference. The adiabatic VBM (not listed in Table 4) is equal to the vertical VBM within the statistical accuracy of the calculation ($\approx$0.1 V). Evidently, the response of the liquid to the introduction of a hole is minimal, at least at the GGA level of theory. This is far from what happens in reality. Ionization of water is rapidly followed by production of hydroxyl radicals, aqueous protons and solvated electrons.[123] The failure of the GGA to localize holes is closely related to the underestimation of the IP. The reason is the massive overstabilization of delocalized holes. Indeed application of HSE leads to localization and is even capable to account for the ensuing separation of charge and spin as has been shown by Marsalek *et al.*[125]

8 Pt(111) at zero electronic charge

Energy level diagrams are a most informative visualization of the effect of interface potentials. With the data of Table 4 we can construct such a diagram for the Pt water interface at the potential of zero charge. The result is shown in Fig. 6. The vacuum level just outside the Pt electrode has been obtained by adding the workfunction of the bare metal to the Fermi level of the aqueous electrode (see Fig. 2). For the U_{VBM} of liquid water Table 4 offers the choice of either the vertical IP or the HOMO energy. The level in the figure corresponds to the IP. The vacuum level of water relative to the SHE is set to the negative of the absolute SHE potential (4.44 V). The argument given in the electrochemistry literature for treating the potential just outside the surface of electrolytic solutions as an absolute zero is that surface charges of water are negligible even at finite concentrations of ionic solutes. We have also added the $OH^{\bullet}/OH^{-}$ and $OH^{\bullet}/H_2O$ redox levels from Table 3. Recall that these levels represent standard reduction potentials of hydroxyl radicals in homogeneous solution without any interaction with metal electrodes.

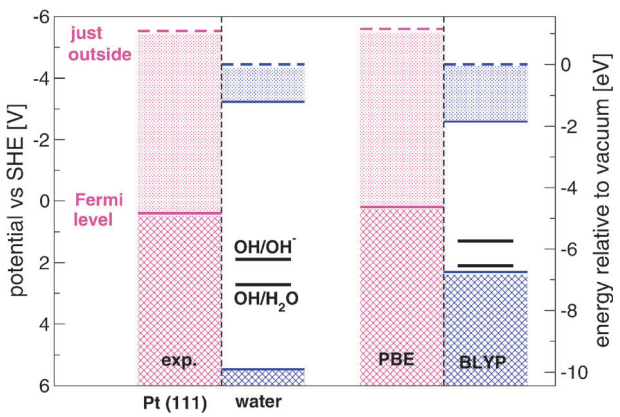

Fig. 6 Level alignment at the Pt(111)–water interface (pH 0) at the potential of zero charge. Pt and liquid water levels are from Table 4, the $OH^{\bullet}$ reduction potentials from Table 3.

The striking contrast in performance of the GGA in placing the Fermi level of Pt and the VBM of liquid water is clearly brought out in Fig. 6. The GGA does very well for one-electron energies of Pt and fails rather badly for water. The favourable Pt result could have been anticipated from the large body of work by the computational surface community. However, the Fermi level in Fig. 6 has been shifted by the interaction with water. This is evident from the positive value (+1.1 V) of the vacuum level of the electrode on the absolute vacuum scale. The step down from Pt to water is the contact potential (Volta potential difference) as discussed in Section 2.2. PBE is evidently capable of accounting quantitatively for the surface potential due to the ordering of water at the interface with the metal. Also the virtual levels of water start from approximately the correct energy. The occupied states are however pushed up way too high by the GGA (BLYP). From a practical perspective one can argue that since the Fermi level of the metal electrode is properly aligned with the SHE, all that matters is a sufficiently large separation in energy from the VBM of water. However at the reversible potential for the oxygen reduction reaction (1.2 V) the GGA leaves only a gap of 0.8 eV between the Pt Fermi level and the water HOMO, which could lead to spurious interactions. In fact we will argue that the underestimation of the reduction potential of $OH^{\bullet}$ is a manifestation of the VBM of water coming too close in energy (see the evaluation in Section 10).

9 Rutile TiO_2(110) at zero proton charge

9.1 Overview of experimental data

Electrochemical interfaces formed by transition metal oxides are a step up in complexity compared to metal electrodes.[126,127] The electronic structure of transition metal oxides can vary from metallic (RuO_2, IrO_2) and near metallic (MnO_2) to semiconducting (TiO_2, Fe_2O_3, Co_3O_4). The gap can be small with the conductivity determined by free charge carriers or the gap can be large in which case the conductivity is mostly polaronic. Some of the metallic compounds are powerful electrocatalysts (for example RuO_2).[73–76] Wide gap semiconductors are applied in photocatalysis.[128,129] Similar to metallic electrodes, the electrochemical activity is due to exchange of electrons with redox couples in solution or redox active surface species. However, the carrier densities in semiconducting electrodes are much lower than in metals. The mobile charge density in the solid is also lower than the ionic charge density in the electrolytic solutions of an ionic strength of interest in applications. The result is that the potential gradient in a double later is partly (or even mainly) on the solid side of the interface. In doped semiconductors this leads to build up of space charge layers and band bending.[126,127]

A second distinction with metals is the acid–base activity of transition metal oxides. The partly ionic character enhances the acidity of adsorbed water. Exposed surface oxygens can act as basic sites attracting protons. This leads not only to dissociative adsorption of water and hydroxylation of the surface but also to exchange of protons with the electrolytic solution. Depending on the pH the surface donates or accepts protons acquiring a net surface charge in the process. The excess surface

charge is compensated by ions in solution. The potential gradients across these ionic double layers can be substantial and are manifested in pH dependence of the electronic band edges.[130] Proton exchange also plays a key role in the electro and photo catalytic activity of transition metal oxides. The coupling to electron exchange ensures that the multiple oxidation states of transition metal centers are accessible in a relatively narrow electrode potential window. Capturing this unique behaviour is an strong argument in favour of hydrogen insertion methods.

Titanium oxide (TiO_2) is the benchmark transition metal oxide exhibiting all of the above-mentioned properties of wide gap semiconductors. It is an extremely popular system, both in experiment and computation, and the literature on TiO_2 is absolutely huge. Here we quote only a couple of key experimental papers[130–133] and a very small selection of computational papers of direct relevance to the discussion.[21,25,59–62,134–138] For an extensive bibliography we can only direct the reader to recent reviews.[128,129]

Titania was therefore an obvious first choice for the application of our hydrogen insertion scheme. To validate the method we have computed some of the characteristic properties of the rutile TiO_2(110) water interface.[65,66,77] In these first applications we have avoided the full complexity of the electric double layer and restricted the calculations to the special state point where there is no net electronic or protonic charge. This special state can also be realized in experiment. The space charge layer can be eliminated by the application of an appropriate bias, the flatband potential (FBP), which can be determined from capacitance measurements.[130] The CBM of TiO_2 electrodes practically coincides with the Fermi level within 0.1 eV.[131] The FBP can therefore be regarded as an estimate of the CBM free of space charge effects. The surface potential controlled by proton exchange can be minimized by measuring the FBP at the pH of the point of zero net proton charge (PZPC). The PZPC of TiO_2 rutile (110) is about 5. At this pH the FBP is at −0.25 V *versus* SHE[130] with the CBM at U_{CBM} = −0.35 V or 4.10 eV below absolute vacuum.[132] The bandgap is effectively insensitive to applied voltage or pH. Ref. 132 uses the value of ΔE_g = 3.0 eV placing the valence band edge at U_{VBM} = 2.65V *vs.* SHE or −7.10 eV on the vacuum scale. Comparing again to the VMB of the clean surface in vacuum should give us a measure of the surface potential created by hydration in solution. The energy of the VBM under vacuum conditions has been the subject of some uncertainty. We will rely on recent experiments by Onda and Petek[133] which place the VBM in vacuum at −8.5 eV, 1.4 eV lower than the VBM at PZCP. The experimental data reviewed above have been summarized in Table 4 and are shown in the form of a level diagram in Fig. 7.

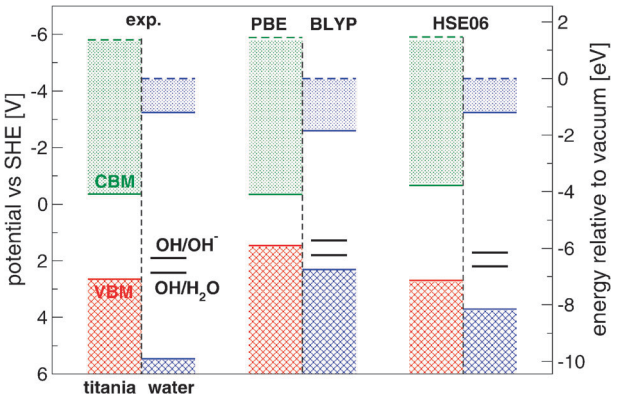

Fig. 7 Level alignment at the rutile TiO_2(110)–water interface at the point of zero proton charge (pH 5) and zero electronic charge (flatband potential). TiO_2 and liquid water levels are from Table 4, the $OH^{\bullet}$ reduction potentials from Table 3.

9.2 Definition and preparation of model system

Computational investigations of the band structure of titania have been reported in numerous publications.[25,59–61,134–138] Band offset calculations at semiconductor liquid interfaces are more rare and are all based on a comparison of the density of states of the solid and the liquid (see for example ref. 25 and 59). In our previous studies on the rutile TiO_2(110)–water interface we have taken a more electrochemical view aligning the energy levels w.r.t the SHE.[65,66] The results obtained using PBE are summarized in Table 4 and represented in the level diagram of Fig. 7. The TiO_2 model system had the alternating solid water slab geometry shown schematically in Fig. 4. The system was set up as a solid slab of stoichiometric TiO_2 in contact with a volume of pure liquid water (no ions). This model semiconductor–water interface is indicated as TiO_2(aq) in Table 4.

We investigated two systems of different size. The TiO_2 slab of ref. 66 and 67 consisted of five O–Ti–O trilayers (5 L) with the *xy* dimensions of 4 × 2 supercell (80 formula units of TiO_2 in total). The slab is replicated along the *z*-axis with a 15 Å gap between periodic images. The gap was filled with 71 water molecules. The overall dimensions of the orthorhombic cell are 11.9 × 13.2 × 30.8 $Å^3$ (For a molecular graphics representation see Fig. 1 of ref. 66). The system used in the first application of our level alignment method in ref. 65 was smaller. The size of the MD cell was 11.9 × 13.2 × 24.2 $Å^3$ containing a TiO_2 slab of only 3 O–Ti–O trilayers (3 L). The number of H_2O molecules (71) was the same. The GGA used was PBE. Some of the 5 L calculations were repeated using HSE06. Because of the increased costs of an exact exchange hybrid functional only TiO_2 slabs covered with one monolayer (ML) of water were considered.

Water was found to adsorb in the molecular form on the five layer (5 L) system. Dissociation events (or rather attempts) were rare during the length of the simulation (10–20 ps). There is effectively no exchange of protons between the hydrated slab and the solution. Neither did we observe any electron exchange (as expected). The total number of electrons and protons is fixed in DFTMD simulation. On the basis of the arguments given in the review of experimental data we claim therefore that the energy levels of the DFTMD model system under fixed zero charge conditions can be compared to the experimental flatband levels at pH 5. However, reducing the number of TiO_2 makes a clear difference. Dissociation of adsorbed water on the three layer (3 L) slab was much easier. This was the fate of on average 25% of the water molecules leading to on average 25% of the undercoordinated Ti sites occupied by an hydroxide group with a proton bound to a

neighbouring bridging oxygen.[77] Sensitivity of energetics and even geometry to the number of layers is well documented for TiO_2 slabs in vacuum.[134,135] This must also be the explanation for our observations although we have the impression that the effect for an aqueous slab is less serious than for a dry slab. Also for the 3 L system transfer of protons to the solvent was negligible.

9.3 Band alignment using the hydrogen insertion method

The scheme for alignment of the HOMO and LUMO is the least involved and a convenient starting point for the discussion of the results in Table 4. The procedure is an application of the half reaction scheme and was already used for water in Section 7.2. The calculation was carried out for the 3 L system in ref. 65. The uncorrected (raw) HOMO and LUMO energies are 1.29 and 3.09 eV, respectively. Evidently, the bias in the electrostatic potential in the supercell, referred to as V_0 of Section 5, has shifted the orbitals to positive energies. The V_0 effect is cancelled by the bias in the adiabatic deprotonation energy of a hydronium ion ($\Delta_{dp}A_{H_3O^+}$). This quantity is highly composition specific. It is therefore absolutely crucial that the hydronium is solvated in the liquid between two solid slabs in the model for which we want to compute the energy levels. To emphasize this point, we quote the result for the 3 L system given in ref. 65. The insertion energy, $\Delta_{dp}A_{H_3O^+} = 18.91$ eV, is 3.6 eV more than for liquid water (last row of Table 3). Even the difference in the ratio solid liquid in the 5 L compared to the 3 L system will be sufficient to cause significant change in the bias. Substituting the negative of the orbital energies in eqn. (46) and (47) yields $U_{VBM} = 1.46$ V and $U_{CBM} = -0.34$ V as listed Table 4. The small inconsistency with the energies given in ref. 65 is due to a change of mind about the thermodynamic status of the model hydronium ion in our method as explained in ref. 81.

Table 4 also includes band edge positions for the aqueous interface obtained from total energy differences. These states are not vertical, but adiabatic levels determined by removal or insertion of an electron proton pair in the full reaction scheme (see Section 4.3). The thermodynamic integrals are again taken form ref. 65. With these data as input U_{VBM} was recomputed according to eqn (42) and U_{CBM} according to eqn (45). The pK_W needed for the evaluation of U_{VBM} is taken from Table 3 (In ref. 65 we used the experimental value). The discrepancy between the total energy and orbital estimates is not significant in view of the limited accuracy in the calculation and our conclusion is that the two agree. We made a similar observation for water as discussed at the end of Section 7.2. Agreement between the adiabatic and vertical IP for solids is less of a surprise than it is for water, because the atomic relaxation in response to ionization can be expected to be less severe. However, also in metal oxides localization of valence band holes is a well-known phenomenon and is of great importance in applications in electronics and photovoltaics. Also holes in valence bands of TiO_2 are self-trapped as we verified in ref. 66 applying the HSE06 functional instead of PBE. Again, as for water, the (near) coincidence of vertical and adiabatic levels is an artefact of the GGA caused by the delocalization error.

The discussion sofar was restricted to the 3 L system. The 5 L system was studied in ref. 66 in an investigation of the oxidative dehydrogenation of a H_2O molecule adsorbed at the rutile (110) interface with water. The focus was on the thermochemistry of this reaction, which is the first step in the four electron oxidation of water. Band edge potentials were not computed in ref. 66, at least not for the fully solvated surface (see below). In the special case of the GGA, however, we can still extract a band edge potential from the reaction free energies exploiting the inherent flaws in the GGA already noticed. The reaction for estimation of U_{VBM} is oxidation of an adsorbed OH^- group with a surface hydroxyl as product

$$TiOH^- + H^+(aq) \rightarrow TiOH^\bullet + \tfrac{1}{2}H_2 \qquad (67)$$

where Ti stands for a five-fold coordinated Ti^{4+} surface site. The free energy was evaluated by simultaneous desolvation of the aqueous proton and elimination of an electron from the TiO_2 subsystem.[66] The result is a system with an unpaired electron and it is easy to see where the hole resides from the spindensity (see Fig. 1 in ref. 66). The hole in the PBE system was not at all on the surface hydroxyl as suggested in eqn (67), but was delocalized over the oxygen atoms of the TiO_2 slab implying that the electron was taken not from the hydroxide but from the valence band. If that is the case, the free energy change of reaction (67) should be equal to the adiabatic U_{VBM}, provided that the residual interaction between delocalized hole and surface hydroxide can be ignored. This is how the value (1.28 V) for U_{VBM} for the 5 L aqueous system in Table 4 was obtained.

The cathodic complement of reaction (67) is reduction of a protonated bridging oxygen. Indicating this hydronium-like species by Ti_2OH^+ the reaction is written as

$$Ti_2OH^+ + OH^-(aq) + \tfrac{1}{2}H_2 \rightarrow Ti_2OH^\bullet + H_2O \qquad (68)$$

The product is also a surface hydroxyl group which should be distinguished from the one of reaction (67). However, again PBE fails to deliver. The electron is picked up by the conduction band and the free energy of reaction (68) can be used as an estimate of the potential of the CBM *vs.* the SHE after correction for the water dissociation constant. The result (−0.27 V) is listed in Table 4 as the U_{CBM} of the 5 L aqueous surface. U_{VBM} and U_{CBM} obtained through this indirect route are on the low side (in absolute value). The bandgap (1.55 eV) is 0.5 eV smaller than the adiabatic gap we found for the 3 L system. This is a combination of two finite system size effects. Part of the error is due to the difference in thickness of the TiO_2 slab (z direction) and part of it to the limited extension parallel to the surface (x, y directions). Coulombic interactions between a delocalized valence band hole and the charged surface group carried over from the reactant, *i.e.* the adsorbed hydroxide in eqn (67) vanish in the limit of large lateral supercell dimensions. The same holds for interactions between conduction band electrons and the adsorbed proton in eqn (68). For small supercells these interactions are finite. This error is unique to the indirect scheme based on eqn (67) and (68). All other results in Table 4 are not affected. The indirect scheme is clearly not the preferred method for computing U_{VBM} and U_{CBM}. It is however instructive, if only as an illustration of what can go wrong in a GGA calculation.

Application of the HSE06 functional makes a qualitative difference. Switching from PBE to HSE06 during a DFTMD

run of the ionized aqueous TiO_2 slab localizes the hole within a few hundred femto second.[66] Evidently the 25% or so fraction of exact exchange in hybrid functionals is sufficient to stabilize self-trapped holes in the O2p band of TiO_2 as has also been observed in work by other authors.[136–138] What is of interest in the present context however is the energy of the unstable delocalized holes in the valence band. *i.e.* the vertical IP of aqueous TiO_2. Aligning the vertical IP relative to the SHE according to the rules of the hydrogen insertion method requires computation of the solvation free energy of the proton in the same model system. For pure liquid water this computation is feasible at the HSE06 level and the results are discussed in Section 7.2. However the supercell used to model the interface is more than three times larger counting the number of oxygen ions. For a system of this size DFTMD sampling of solvent fluctuations under exact exchange is still very demanding. The workfunction method is much more efficient and fortunately gives fairly accurate results for TiO_2. Titania is a metal oxide with strongly hydrophilic surfaces. It turns out that a static calculation of a slab covered with a single monolayer (ML) of adsorbed water can account for most of the solvation shift in the band positions. Sampling is not necessary (in contrast to the effectively hydrophobic Pt surface). We showed this in ref. 65 for the 3 L system for which a complete set of data is available. These data have been summarized in Table 4. The calculation was repeated for the 5 L system and the results can also be read from Table 4. U_{VBM} in the HSE06 approximation is almost in perfect agreement with experiment. U_{CBM} is somewhat too negative but not too much.

The key results for the TiO_2–water interface are displayed in the level diagram of Fig. 7. To represent the GGA calculation we have selected the HOMO and LUMO energies of the 3 L aqueous system. The TiO_2 levels in the HSE06 panel are for the TiO_2(5 L)–H_2O(1 ML) system. The water levels are the same as in Fig. 6. Also the $OH^{\bullet}/OH^{-}$ and $OH^{\bullet}/H_2O$ redox levels have been inserted again. Regarding the GGA calculation the message is that, as for water, the VBM lies is too high, while the CBM is approximately at the correct energy. Other than this, the semiconductor–water interface diagram is consistent with the one for the metal: the severe underestimation of the IP of liquid water lifts up the HOMO of water bringing it too close to the HOMO of the electrode. The parallel between the semiconductor and the metal is even stricter when TiO_2 is treated in the HSE06 approximation, because now, also the VBM is correctly aligned with the SHE as is the Fermi level of the metal in the GGA. Note, however, that the interface potential is in good agreement with experiment both for the GGA and HSE06 as can be deduced from the alignment of the TiO_2 vacuum level. This observation is consistent with the results for the acidity of adsorbed water in ref. 66. The change of functional had little effect on the pK.

10 Evaluation and outlook

The very different nature of metals, semiconductors and electrolytic solutions makes the calculation of potentials at electrochemical interfaces particularly hard. The problem seems simpler for reversible electrodes. Electrochemical equilibrium between phases equalizes the Fermi levels. Computation of potentials of reversible electrodes becomes a question of computing reaction free energies in the bulk or chemisorption energies at a surface (Nernst law). The focus in this perspective has been on methods for calculating potentials of ideally polarizable interfaces which are impossible to cross for electrons. The methods are however also relevant for reversible electrodes. Similar questions arise when one wants to know how much charge has been exchanged.

The central electrochemical formalism underlying the computation of potentials of electrochemically inactive electrodes is the modern theory of absolute electrode potentials. Potentials of single electrodes are identified with electronic workfunctions.[4,68] This definition applies to reversible as well as ideally polarizable electrodes because the work for transferring electrons to vacuum is defined whether there is electron exchange between the electrode and electrolytic solution or not. Electronic energy levels can be interpreted as ionization potentials or electron affinities (or both in the case of metals). The theory of absolute electrode potentials is therefore also the key to aligning electronic energy levels with respect to the standard hydrogen electrode. We looked at two examples, namely the level diagram for the Pt(111)–water interface at pH 0 (Fig. 6) and the rutile TiO_2(110)–water interface at pH 5 (Fig. 7).

The presentation was restricted to all-atom methods treating the solvent at the same level of theory as the solid. Two such methods were selected for discussion, the explicit solvent implementation of the workfunction method[38,55] and the hydrogen insertion method[54,65] which is inherently all-atom. Explicit modelling of the solvent becomes necessary when electrode potentials are sensitive to fluctuations in the solvent. The potential of zero charge of the Pt(111) is an example of such a system which in principle requires statistical sampling. Sampling comes at a massive increase in the cost of the calculation and considerable effort has been spent on trying to avoid it, even in explicit solvent models.[55] In this context, it should perhaps be stressed that sampling, while expensive, is feasible at the current stage of technology (at least at the level of the GGA) as the two examples in the perspective show. A related issue for all-atom methods is of course the limitation in the system size. This is a serious drawback preventing the application of explicit solvent models at low ionic strength. The reason is the large extension of the diffuse layer as studies using implicit solvent models never fail to mention.[25,28] However, many reactions of interest in electrocatalysis require high potentials (H_2O oxidation) or low potentials (CO_2 reduction). Almost all of the drop in potential under these conditions is over the compact (Helmholtz) double layer which can be (and probably must be) represented by explicit solvent models.

A good fraction of this review is devoted to a derivation of the workfunction and hydrogen insertion method from the theory of absolute electrode potentials. The workfunction method has its origin in computational surface science and can be regarded as the most direct application of the concept of an absolute electrode potential referred to vacuum. The hydrogen insertion method uses the solvation free energy of a proton as energy reference and therefore resembles an electrochemical cell with the hydrogen electrode as a reference electrode.

The detour through vacuum seems unnecessary. However, it proved to be a convenient route to provide a firm electrochemical basis for the calculation of potentials of ideally polarizable electrodes in the framework of the hydrogen insertion method. It also enabled us to make a clear connection to the workfunction function method.

Compared to the workfunction method, the hydrogen insertion method is significantly more involved and expensive. Sampling is not an option but mandatory, because the computation must account for the large reorganization of the solvent induced by reduction of an aqueous proton.[139] The advantage of this fundamentalistic approach is that the hydrogen insertion method can also be used to compute reversible electrode potentials of homogeneous redox reactions as well as the free energy for proton transfer which is not a Faradaic process at all. This feature allows us to resolve a dehydrogenation reaction in a deprotonation and oxidation, which was crucial in our recent study of the oxidative dehydrogenation of water adsorbed on an aqueous TiO_2 electrode. We showed that the catalytic effect of adsorption is almost entirely due to the activation of the acidity of water by the ionic surface and not to a decrease of the oxidation potential.[66]

The unified treatment of heterogeneous and homogeneous redox reactions is also what led us to the main message of this perspective for the application of DFT methods to electrocatalysis. This is the danger posed by the huge underestimation of the vertical ionization potential of liquid water. The same methods do comparatively better for the energy levels of solid electrodes. The result is a narrowing of the gap between the HOMO of water and the HOMO of the electrode, which in some unfavourable cases can bring the valence band of water almost in coincidence with the electroactive levels of the electrode. In fact the same mechanism is active for homogeneous reactions. We now believe that the unrealistic elevated position of the valence band of water is responsible for the underestimation of the reduction potential of the hydroxyl radical as documented in Table 3. If the valence band edge moves up, solute levels in the bandgap have to follow. The effect is larger the closer the solute level is to the valence band of the solvent and therefore particularly serious for highly oxidative species such as the OH radical.[140] This explanation is supported by the superior performance of implicit solvent models in which interactions with extended states of the solvent have been eliminated. Using the same GGA implicit solvent calculations can reproduce redox potentials of reactive radicals within 0.1 V.[27] The errors introduced by an explicit water representation can be relieved to a considerable extent by including an exact exchange component in the functional at the expense of further increase in computational cost. We expect the extra costs to pay off in the study of surface reactions under the harsh conditions in electrical double layers at potentials required to activate stable molecules.

Acknowledgements

Marialore Sulpizi and Joost VandeVondele are acknowledged for their crucial contributions to development and validation of the hydrogen insertion method as reported here. JC is grateful for financial support of Emmanuel College Cambridge and the Engineering and Physical Sciences Research Council (EPSRC) of the United Kingdom. We also acknowledge support from the UKCP consortium for access to HECToR, the UK's high-end computing resource funded by the Research Councils.

References

1 A. J. Bard and L. R. Faulkner, *Electrochemical Methods*, John Wiley & Sons, New York, 2nd edn, 2001.
2 V. S. Bagotsky, *Fundamentals of Electrochemistry*, John Wiley & Sons, Hoboken, New Jersey, 2006.
3 C. H. Hamann, A. Hamnett and W. Vielstich, *Electrochemistry*, Wiley-VCH, Weinheim, 2007.
4 W. R. Fawcett, *Liquids, Solutions, and Interfaces*, Oxford University Press, Oxford, 2004.
5 A. B. Anderson and T. V. Albu, *J. Am. Chem. Soc.*, 1999, **121**, 11855–11863.
6 Y. Cai and A. B. Anderson, *J. Phys. Chem. B*, 2004, **108**, 9829–9833.
7 T. Zhang and A. B. Anderson, *Electrochim. Acta*, 2007, **53**, 982–989.
8 Y. Wang and P. B. Balbuena, *J. Phys. Chem. B*, 2005, **109**, 18902–18906.
9 T. Jacob, *Fuel Cells*, 2006, **6**, 159–181.
10 E. Santos, A. Lundin, M. T. M. Koper and W. Schmickler, *Chem. Phys.*, 2009, **344**, 195–201.
11 E. Santos, A. Lundin, K. Pötting, P. Quaino and W. Schmickler, *Phys. Rev. B: Condens. Matter Mater. Phys.*, 2009, **79**, 235436.
12 F. Wilhelm, W. Schmickler and E. Spohr, *J. Phys.: Condens. Matter*, 2010, **22**, 175001.
13 J. K. Nørskov, J. Rossmeisl, A. Logadottir, L. Lindqvist, J. R. Kitchin, T. Bligaard and H. Jónsson, *J. Phys. Chem. B*, 2004, **108**, 17886–17892.
14 J. Rossmeisl, A. Logadottir and J. K. Nørskov, *Chem. Phys.*, 2005, **319**, 178–184.
15 V. Tripkovíc, E. Skúlason, S. Siahrostami, J. K. Nørskov and J. Rossmeisl, *Electrochim. Acta*, 2010, **55**, 7975–7981.
16 E. Skúlason, V. Tripkovic, M. E. Björketun, S. Gudmundsdóttir, G. Karlberg, J. Rossmeisl, T. Bligaard, H. Jónsson and J. K. Nørskov, *J. Phys. Chem. C*, 2010, **114**, 18182–18197.
17 A. U. Nilekar and M. Mavrikakis, *Surf. Sci.*, 2008, **602**, L89–L94.
18 H.-F. Wang and Z.-P. Liu, *J. Phys. Chem. C*, 2009, **113**, 17502–17508.
19 *Faraday Discussion: Electrocatalysis Theory and Experiment at the Interface*, ed. M. T. M. Koper, 2008, vol. 140.
20 M. T. M. Koper, *J. Electroanal. Chem.*, 2011, **660**, 254–260.
21 J. Rossmeisl, Z.-W. Qu, H. Zhu, G.-J. Kroes and J. K. Nørskov, *J. Electroanal. Chem.*, 2007, **607**, 83–89.
22 A. Vojvodic, F. Calle-Vallejo, W. Guo, S. Wang, A. Toftelund, F. Studt, J. I. Martïnez, J. Shen, J. Rossmeisl, T. Bligaard, J. K. Nørskov and F. Abild-Pedersen, *J. Chem. Phys.*, 2011, **134**, 244509.
23 I. C. Man, H. Y. So, F. Calle-Vallejo, H. A. Hansen, J. I. Martinez, N. G. Inoglu, J. Kitchin, T. F. Jaramillo, J. Rossmeisl and J. K. Nørskov, *ChemCatChem*, 2011, **3**, 1159–1165.
24 A. Valdés, J. Brillet, M. Grätzel, H. Gudmundsdóttir, H. A. Hansen, H. Jónsson, P. Klüpfel, G.-J. Kroes, F. Le Formal, I. C. Man, R. S. Martins, J. K. Nørskov, J. Rossmeisl, K. Sivula, A. Vojvodic and M. Zäch, *Phys. Chem. Chem. Phys.*, 2012, **14**, 49–70.
25 Y.-F. Li, Z.-P. Liu, L. Liu and W. Gao, *J. Am. Chem. Soc.*, 2010, **132**, 13008–13015.
26 Y.-H. Fang and Z.-P. Liu, *J. Am. Chem. Soc.*, 2010, **132**, 18214–18222.
27 R. Jinnouchi and A. B. Anderson, *J. Phys. Chem. C*, 2008, **112**, 8747–8750.
28 R. Jinnouchi and A. B. Anderson, *Phys. Rev. B: Condens. Matter Mater. Phys.*, 2008, **77**, 245417.
29 F. Tian, R. Jinnouchi and A. B. Anderson, *J. Phys. Chem. C*, 2009, **113**, 17484–17492.
30 F. Tan and A. B. Anderson, *J. Phys. Chem. C*, 2011, **115**, 4076–4088.

31 A. B. Anderson, *Phys. Chem. Chem. Phys.*, 2012, **14**, 1130–1338.
32 Y. Sha, T. H. Yu, Y. Liu, B. V. Merinov and W. A. Goddard III, *J. Phys. Chem. Lett.*, 2010, **1**, 856–861.
33 Y. Sha, T. H. Yu, B. V. Merinov, P. Shrivanian and W. A. Goddard III, *J. Phys. Chem. Lett.*, 2011, **2**, 572–576.
34 J.-S. Filhol and M. Neurock, *Angew. Chem., Int. Ed. Engl.*, 2006, **45**, 402–406.
35 C. D. Taylor, S. A. Wasileski, J.-S. Filhol and M. Neurock, *Phys. Rev. B: Condens. Matter Mater. Phys.*, 2006, **73**, 165402.
36 M. Janik, C. D. Taylor and M. Neurock, *J. Electrochem. Soc.*, 2009, **156**, B126–B135.
37 M. Otani and O. Sugino, *Phys. Rev. B: Condens. Matter Mater. Phys.*, 2006, **73**, 115407.
38 M. Otani, I. Hamada, O. Sugino, Y. Morikawa, Y. Okamoto and T. Ikeshoji, *J. Phys. Soc. Jpn.*, 2008, **2**, 024802.
39 Y. Okamoto and O. Sugino, *J. Phys. Chem. C*, 2010, **114**, 4473–4478.
40 R. Guidelli and W. Schmickler, *Electrochim. Acta*, 2000, **43**, 2317–2338.
41 A. A. Kornyshev, *J. Phys. Chem. B*, 2007, **111**, 5545–5557.
42 J. C. Shelley, G. N. Patey, D. R. Bérard and G. M. Torrie, *J. Chem. Phys.*, 1997, **107**, 2122–2141.
43 E. Spohr, *Electrochim. Acta*, 1999, **44**, 1697–1705.
44 A. P. Willard, S. K. Reed, P. A. Madden and D. Chandler, *Faraday Discuss.*, 2009, **141**, 423–441.
45 R. M. Lynden-Bell, M. DelPópolo, T. G. A. Youngs, J. Kohanoff, C. G. Hanke, J. B. Harper and C. C. Pinilla, *Acc. Chem. Res.*, 2007, **40**, 1138–1145.
46 M. V. Fedorov and A. A. Kornyshev, *J. Phys. Chem. B*, 2008, **112**, 11868–11872.
47 S. Tazi, M. Salanne, C. Simon, P. Turq, M. Pounds and P. Madden, *J. Phys. Chem. B*, 2010, **114**, 8453–8459.
48 J. Vatamanu, O. Borodin and G. D. Smith, *J. Am. Chem. Soc.*, 2010, **132**, 14825–14833.
49 W. Schmickler, *Chem. Rev.*, 1996, **96**, 3177–3200.
50 *Chemical bonding at surfaces and interfaces*, ed. A. Nilsson, L. G. M. Petterson and J. K. Nørskov, Elsevier, Amsterdam, 2008.
51 C. P. Kelly, C. J. Cramer and D. Truhlar, *J. Phys. Chem. B*, 2006, **110**, 16066–16081.
52 C. P. Kelly, C. J. Cramer and D. Truhlar, *J. Phys. Chem. B*, 2007, **111**, 408–422.
53 A. A. Isse and A. Gennaro, *J. Phys. Chem. B*, 2010, **114**, 7894–7899.
54 J. Rossmeisl, E. Skúlason, M. E. Björketun, V. Tripkovic and J. K. Nørskov, *Chem. Phys. Lett.*, 2008, **466**, 68–71.
55 V. Tripkovic, M. E. Björketun, E. Skúlason and J. Rossmeisl, *Phys. Rev. B: Condens. Matter Mater. Phys.*, 2011, **84**, 115452.
56 S. Schnur and A. Gross, *New J. Phys.*, 2009, **11**, 125003.
57 S. Schnur and A. Gross, *Catal. Today*, 2011, **11**, 129–137.
58 X. Shen, Y. A. Small, J. Wang, P. B. Allen, M. V. Fernandez-Serra, M. S. Hybertsen and J. T. Muckerman, *J. Phys. Chem. C*, 2010, **114**, 13695–13704.
59 H. Cheng and A. Selloni, *Langmuir*, 2010, **26**, 11518–11525.
60 M. Sumita, C. Hu and Y. Tateyama, *J. Phys. Chem. C*, 2010, **114**, 18529–18537.
61 F. Schiffmann, J. VandeVondele, J. Hutter, A. Urakawa, R. Wirz and A. Baiker, *Proc. Natl. Acad. Sci. U. S. A.*, 2010, **107**, 4830–4833.
62 F. De Angelis, S. Fantacci and R. Gebauer, *J. Phys. Chem. Lett.*, 2011, **2**, 813–817.
63 T. Ikeda, M. Boero, S.-F. Huang, K. Terakura, M. Oshima, J.-I. Ozaki and S. Miyata, *J. Phys. Chem. C*, 2010, **114**, 8933–8937.
64 Y. Wu, M. K. Y. Chan and G. Ceder, *Phys. Rev. B: Condens. Matter Mater. Phys.*, 2011, **83**, 235301.
65 J. Cheng and M. Sprik, *Phys. Rev. B: Condens. Matter Mater. Phys.*, 2010, **82**, 081406(R).
66 J. Cheng, M. Sulpizi, J. Joost VandeVondele and M. Sprik, *ChemCatChem*, 2012, **4**, 636–640.
67 S. Trasatti, *J. Electroanal. Chem.*, 1982, **139**, 1–13.
68 S. Trasatti, *Pure Appl. Chem.*, 1986, **58**, 955–966.
69 S. Trasatti, *Electrochim. Acta*, 1990, **35**, 269–271.
70 S. Trasatti, *Electrochim. Acta*, 1991, **36**, 1659–1667.
71 S. Trasatti, *Surf. Sci.*, 1995, **335**, 1–9.
72 W. R. Fawcett, *Langmuir*, 2008, **24**, 9868–9875.
73 S. Trasatti, *J. Electroanal. Chem.*, 1980, **111**, 125–131.
74 S. Trasatti, *Electrochim. Acta*, 1991, **36**, 225–241.
75 S. Ardizzone and S. Trasatti, *Adv. Colloid Interface Sci.*, 1996, **64**, 173–251.
76 E. Guerrini and S. Trasatti, *Russ. J. Electrochem.*, 2006, **225**, 1131–1140.
77 J. Cheng and M. Sprik, *J. Chem. Theory Comput.*, 2010, **6**, 880–889.
78 E. Gileadi, *J. Solid State Electrochem.*, 2011, **15**, 1359–1371.
79 C. Adriaanse, M. Sulpizi, J. VandeVondele and M. Sprik, *J. Am. Chem. Soc.*, 2009, **131**, 6046–6047.
80 J. Cheng, M. Sulpizi and M. Sprik, *J. Chem. Phys.*, 2009, **131**, 154504.
81 F. Costanzo, R. G. Della Valle, M. Sulpizi and M. Sprik, *J. Chem. Phys.*, 2011, **134**, 244508.
82 G. King and A. Warshel, *J. Chem. Phys.*, 1990, **93**, 8682.
83 F. S. Lee, Z. T. Chu, M. B. Bolger and A. Warshel, *Protein Eng.*, 1992, **5**, 215.
84 A. D. Becke, *Phys. Rev. A: At., Mol., Opt. Phys.*, 1988, **38**, 3098.
85 C. Lee, W. Yang and R. Parr, *Phys. Rev. B: Condens. Matter Mater. Phys.*, 1988, **37**, 785.
86 J. P. Perdew, K. Burke and M. Ernzerhof, *Phys. Rev. Lett.*, 1996, **77**, 3865.
87 M. Marsman, J. Paier, A. Stroppa and G. Kresse, *J. Phys.: Condens. Matter*, 2008, **20**, 064201.
88 P. Mori-Sánchez, A. J. Cohen and W. Yang, *Phys. Rev. Lett.*, 2008, **100**, 146401.
89 A. J. Cohen, P. Mori-Sánchez and W. Yang, *Chem. Rev.*, 2012, **112**, 289–320.
90 J. P. Perdew, A. Ruzsinszky, L. A. Constantin, J. Sun and G. I. Csonka, *J. Chem. Theory Comput.*, 2009, **5**, 902–908.
91 A. V. Krukau, O. A. Vydrov, A. F. Izmaylov and G. E. Scuseria, *J. Chem. Phys.*, 2006, **125**, 224106.
92 M. Guidon, J. Hutter and J. VandeVondele, *J. Chem. Theory Comput.*, 2010, **6**, 2348–2364.
93 T. L. Beck, M. E. Paulitis and L. R. Pratt, *The Potential Distribution Theorem and Models of Molecular Solutions*, Cambridge University Press, Cambridge, 2006.
94 B. A. Pethica, *Phys. Chem. Chem. Phys.*, 2007, **9**, 6253–6262.
95 M. H. Tissandier, K. A. Cowen, W. Y. Feng, E. Gundlach, M. H. Cohen, A. D. Earhart and J. V. Coe, *J. Phys. Chem. A*, 1998, **102**, 7787–7794.
96 P. Hunt and M. Sprik, *Comput. Phys. Commun.*, 2005, **6**, 1805.
97 K. Leung, *J. Phys. Chem. Lett.*, 2010, **1**, 496–499.
98 S. M. Kathmann, J. Kuo, C. J. Mundy and G. K. Schenter, *J. Phys. Chem. B*, 2011, **115**, 4369–4377.
99 D. M. Stanbury, *Adv. Inorg. Chem.*, 1989, **33**, 69–138.
100 L. Bengtsson, *Phys. Rev. B: Condens. Matter Mater. Phys.*, 1999, **59**, 12301–12304.
101 L. Yu, V. Ranjan, W. lu, J. Bernholc and M. B. Nardelli, *Phys. Rev. B: Condens. Matter Mater. Phys.*, 2008, **77**, 245102.
102 A. Franciosi and C. G. VandeWalle, *Surf. Sci. Rep.*, 1996, **25**, 1–140.
103 J. Junquera, M. H. Cohen and K. M. Rabe, *J. Phys.: Condens. Matter*, 2007, **19**, 213203.
104 L. Kleinman, *Phys. Rev. B: Condens. Matter Mater. Phys.*, 1981, **24**, 7412.
105 J. J. Warren, T. A. Tronic and J. M. Mayer, *Chem. Rev.*, 2010, **110**, 6961–7001.
106 M.-P. Gaigeot, M. Sprik and M. Sulpizi, *J. Phys.: Condens. Matter*, 2012, **24**, 124106.
107 M. Sulpizi, M.-P. Gaigeot and M. Sprik, *J. Chem. Theory Comput.*, 2012, **8**, 137–147.
108 J. Blumberger, I. Tavernelli, M. L. Klein and M. Sprik, *J. Chem. Phys.*, 2006, **124**, 064507.
109 R. A. Marcus, *Rev. Mod. Phys.*, 1993, **65**, 599–610.
110 M. Sulpizi and M. Sprik, *Phys. Chem. Chem. Phys.*, 2008, **10**, 5238–5249.
111 B. Winter, M. Faubel, I. V. Hertel, C. Pettenkofer, S. E. Bradforth, B. Jagoda-Cwiklik, L. Cwiklik and P. Jungwirth, *J. Am. Chem. Soc.*, 2006, **128**, 3864–3865.
112 R. Seidel, S. Thümer and B. Winter, *J. Phys. Chem. Lett.*, 2011, **2**, 633–641.
113 J. E. Davies, N. L. Doltsinis, A. J. Kirby, C. D. Roussev and M. Sprik, *J. Am. Chem. Soc.*, 2002, **124**, 6594.

114 K. Leung, I. M. B. Nielson and L. J. Criscenti, *J. Am. Chem. Soc.*, 2009, **131**, 18358–18365.
115 R. Ayala and M. Sprik, *J. Phys. Chem. B*, 2008, **112**, 257–269.
116 M. Mangold, L. Rolland, F. Costanzo, M. Sprik, M. Sulpizi and J. Blumberger, *J. Chem. Theory Comput.*, 2011, **7**, 1951–1961.
117 The CP2K developers group, http://cp2k.berlios.de, 2008.
118 J. VandeVondele, M. Krack, F. Mohamed, M. Parrinello, T. Chassaing and J. Hutter, *Comput. Phys. Commun.*, 2005, **167**, 103–128.
119 A. Bernas, C. Ferradini and J.-P. Jay-Gerin, *Chem. Phys.*, 1997, **222**, 151–160.
120 D. Prendergast, J. C. Grossman and G. Galli, *J. Chem. Phys.*, 2005, **123**, 014501.
121 D. Lu, F. Gygi and G. Galli, *Phys. Rev. Lett.*, 2008, **100**, 147601.
122 V. Garbuio, M. Cascella, L. Reining, R. D. Sole and O. Pulci, *Phys. Rev. Lett.*, 2006, **97**, 137402.
123 J. V. Coe, A. D. Earhart, M. H. Cohen, G. J. Hoffman, H. W. Sarkas and K. H. Bowen, *J. Chem. Phys.*, 1997, **107**, 6023–6031.
124 D. P. Chong, O. V. Gritsenko and E. J. Baerends, *J. Chem. Phys.*, 2002, **116**, 1760–1772.
125 O. Marsalek, C. G. Elles, P. A. Pieniazek, E. Pluharova, J. VandeVondele, S. E. Bradforth and P. Jungwirth, *J. Chem. Phys.*, 2011, **135**, 224510.
126 H. Gerischer, *Electrochim. Acta*, 1990, **35**, 1677–1699.
127 A. J. Nozik and R. Memming, *J. Phys. Chem.*, 1996, **100**, 13061–13078.
128 A. Fujishima, X. Zhang and D. A. Tryk, *Surf. Sci. Rep.*, 2008, **63**, 515–582.
129 M. A. Henderson, *Surf. Sci. Rep.*, 2011, **66**, 185–297.
130 l. Kavan, M. Grätzel, S. E. Gilbert and K. C. H. J. Scheel, *J. Am. Chem. Soc.*, 1996, **118**, 6716.
131 N. Sato, *Electrochemistry at metal and semiconductor electrodes*, Elsevier Science & Technology, Oxford, 1998.
132 M. Grätzel, *Nature*, 2001, **414**, 338.
133 K. Onda, B. Li and H. Petek, *Phys. Rev. B: Condens. Matter Mater. Phys.*, 2004, **70**, 045415.
134 P. M. Kowalski, B. Meyer and D. Marx, *Phys. Rev. B: Condens. Matter Mater. Phys.*, 2009, **79**, 115410.
135 L.-M. Liu and A. Michaelides, *Phys. Rev. B: Condens. Matter Mater. Phys.*, 2010, **82**, 161415(R).
136 A. Valdés and G.-J. Kroes, *J. Phys. Chem. C*, 2010, **114**, 1701–1708.
137 C. Di Valentin and A. Selloni, *J. Phys. Chem. Lett.*, 2011, **2**, 2223–2228.
138 T. Yamamoto and T. Ohno, *Phys. Chem. Chem. Phys.*, 2012, **14**, 589–598.
139 This has not always been appreciated. For example it is ignored by Wu *et al.*[64] introducing a significant bias in their level allignment scheme.
140 In ref. 79 we attributed this effect to self-interaction specific to the hydroxyl radical. We now no longer support this picture. This will be worked out in more detail in a future publication.